JGR Atmospheres

RESEARCH ARTICLE
10.1029/2018JD029151

Key Points:
- Korean sources contribute 6-13% to CO along DC-8 flight tracks, while contributions of different East Asian subregions vary from 5% to 28%
- Middle East Asian sources dominate (up to 64%) continental outflows to Korea, but Korean emissions are more important for CO near surface
- Contributions using CAM-chem tags agree with FLEXPART-WRF back trajectories, WRF NO2 inert tracers, China signature VOCs, and CO/CO2

Supporting Information:
- Supporting information S1

Correspondence to:
W. Tang,
wenfutang@email.arizona.edu

Citation:
Tang, W., Emmons, L. K., Arellano Jr, A. F., Gaubert, B., Knote, C., Tilmes, S., et al. (2019). Source contributions to carbon monoxide concentrations during KORUS-AQ based on CAM-chem model applications. *Journal of Geophysical Research: Atmospheres*, *124*, 2796–2822. https://doi.org/10.1029/2018JD029151

Received 10 JUN 2018
Accepted 26 JAN 2019
Accepted article online 1 FEB 2019
Published online 7 MAR 2019

The copyright line for this article was changed on 16 APR 2019 after original online publication.

Source Contributions to Carbon Monoxide Concentrations During KORUS-AQ Based on CAM-chem Model Applications

Wenfu Tang[1], Louisa K. Emmons[2], Avelino F. Arellano Jr[1], Benjamin Gaubert[2], Christoph Knote[3], Simone Tilmes[2], Rebecca R. Buchholz[2], Gabriele G. Pfister[2], Glenn S. Diskin[4], Donald R. Blake[5], Nicola J. Blake[5], Simone Meinardi[5], Joshua P. DiGangi[4], Yonghoon Choi[4,6], Jung-Hun Woo[7], Cenlin He[8], Jason R. Schroeder[4], Inseon Suh[9], Hyo-Jung Lee[10], Hyun-Young Jo[10], Yugo Kanaya[11], Jinsang Jung[12], Youngjae Lee[13], and Danbi Kim[13]

[1]Department of Hydrology and Atmospheric Sciences, University of Arizona, Tucson, AZ, USA, [2]Atmospheric Chemistry Observations and Modeling Laboratory, National Center for Atmospheric Research, Boulder, CO, USA, [3]Meteorologisches Institut, Ludwig-Maximilians-Universität München, Munich, Germany, [4]NASA Langley Research Center, Hampton, VA, USA, [5]Department of Chemistry, University of California, Irvine, CA, USA, [6]Science Systems and Applications, Inc., Hampton, VA, USA, [7]Department of Advanced Technology Fusion, Konkuk University, Seoul, South Korea, [8]Research Applications Laboratory, National Center for Atmospheric Research, Boulder, CO, USA, [9]Department of Earth and Environmental Sciences, Korea University, Seoul, South Korea, [10]Department of Atmospheric Sciences, Pusan National University, Busan, South Korea, [11]Japan Agency for Marine-Earth Science and Technology, Yokosuka, Japan, [12]Korea Research Institute of Standards and Science, Daejeon, South Korea, [13]National Institute of Environmental Research, Incheon, South Korea

Abstract We investigate regional sources contributing to CO during the Korea United States Air Quality (KORUS-AQ) campaign conducted over Korea (1 May to 10 June 2016) using 17 tagged CO simulations from the Community Atmosphere Model with chemistry (CAM-chem). The simulations use three spatial resolutions, three anthropogenic emission inventories, two meteorological fields, and nine emission scenarios. These simulations are evaluated against measurements from the DC-8 aircraft and Measurements Of Pollution In The Troposphere (MOPITT). Results show that simulations using bottom-up emissions are consistently lower (bias: −34 to −39%) and poorer performing (Taylor skill: 0.38–0.61) than simulations using alternative anthropogenic emissions (bias: −6 to −33%; Taylor skill: 0.48–0.86), particularly for enhanced Asian CO and volatile organic compound (VOC) emission scenarios, suggesting underestimation in modeled CO background and emissions in the region. The ranges of source contributions to modeled CO along DC-8 aircraft from Korea and southern (90°E to 123°E, 20°N to 29°N), middle (90°E to 123°E, 29°N to 38.5°N), and northern (90°E to 131.5°E, 38.5°N to 45°N) East Asia (EA) are 6–13%, ~5%, 16–28%, and 9–18%, respectively. CO emissions from middle and northern EA can reach Korea via transport within the boundary layer, whereas those from southern EA are transported to Korea mainly through the free troposphere. Emission contributions from middle EA dominate during continental outflow events (29–51%), while Korean emissions play an overall more important role for ground sites (up to 25–49%) and plumes within the boundary layer (up to 25–44%) in Korea. Finally, comparisons with four other source contribution approaches (FLEXPART 9.1 back trajectory calculations driven by Weather Research and Forecasting (WRF) WRF inert tracer, China signature VOCs, and CO to CO_2 enhancement ratios) show general consistency with CAM-chem.

1. Introduction

Air pollutants and emissions have significant impacts on environment, climate, ecosystem, agriculture, public health, and safety (Charlson et al, 1992; Doney et al., 2007; Feely et al., 2004; Gao et al., 2017; Maher et al., 2016; Ohara et al., 2007; Shindell et al., 2011). This is especially the case in East Asia, where human activities are most intense, accompanied by immense energy consumption (Kennedy et al., 2015). Previous studies have shown that anthropogenic combustion and emissions in East Asia have impacts at both local and hemispheric scales, including long-range transport to North America (Heald et al., 2006; Jacob et al., 1999; Jaffe et al., 1999; Jiang et al., 2016). This highlights an urgent need to better understand emissions and air quality

in East Asia. Field campaigns provide valuable measurements. For example, the NASA Pacific Exploratory Mission in the Western Pacific Ocean Phase B in 1994 studied chemical processes and long-range transport of trace species in Asian outflow over the Northwest Pacific Ocean (Hoell et al., 1997). The NASA Transport and Chemical Evolution over the Pacific was conducted over the Northwest Pacific in 2001 to investigate Asian chemical outflow and its sources and chemical evolution (Jacob et al., 2003). The Asian Pacific Regional Aerosol Characterization Experiments in 2001 aimed to understand the properties and controlling factors of aerosols in the atmosphere of East Asia and the Northwest Pacific (Huebert et al., 2003).

Recently, the Korea United States Air Quality (KORUS-AQ) field measurement campaign was performed based on an international collaboration between United States and South Korea, led by the National Institute of Environmental Research of Korea and the National Aeronautics and Space Administration (NASA) of the United States. The campaign was conducted over South Korea and its surrounding waters in May–June 2016. During the campaign, observations from aircraft, ships, ground sites, and satellites were integrated with models to help understand air quality and factors controlling air quality in the region. The campaign had three main research foci: (1) the opportunities and challenges for satellite observations of air quality, (2) the key factors governing ozone photochemistry and aerosol evolution, and (3) model performance and needed improvements to better represent atmospheric composition over Korea and its connection to the larger global atmosphere (Al-Saadi et al., 2014). To better investigate these research topics, especially (2) and (3), it is critical to understand and quantify the influence of different pollution sources on the air quality in in the region.

Tagging in chemical transport models (CTM) is a powerful tool to investigate source contributions to air pollutants' concentrations levels (Emmons et al., 2012; Granier et al., 1999). The tagging method is particularly appropriate in chemistry by explicitly accounting for nonlinearity in the sensitivity to change in emissions (Clappier et al., 2017). CO is a common pollutant in the atmosphere, being directly emitted from incomplete combustion sources, such as vehicles, industry, and biomass burning, as well as chemically produced from oxidation of methane and other hydrocarbons. CO is also a good tracer of pollution transport, with only one photochemical sink and an intermediate lifetime (approximately a month; Duncan & Bey, 2004; Gamnitzer et al., 2006; Li et al., 2002). Such characteristics make tagging CO feasible and tagged CO relatively reliable as a tracer of pollution plumes from regional to hemispheric scales. Tagged CO has been widely used in previous studies for various research purposes such as source attribution (Buchholz et al., 2016; Chen et al., 2009; Fisher et al., 2017; Granier et al., 1999; Liu et al., 2003; Park et al., 2009; Pfister et al., 2011, 2004; Protonotariou et al., 2013; Staudt et al., 2001) and inverse modeling (Arellano et al., 2004, 2006; Heald et al., 2004; Pétron et al., 2004). Our goal in this study is to elucidate the regional sources contributing to observed CO concentrations within the troposphere over Korea during the KORUS-AQ campaign using the tagged CO algorithm that is implemented in the Community Atmosphere Model with chemistry (CAM-chem).

Despite its wide use in the community, the reliability of source contribution analysis through tagged tracers in CTMs needs further evaluation. Sources apportioned by tagged CO are sensitive to many parameters such as emissions, transport, chemistry, and resolution in the CTM. These factors are important sources of model errors (Gaubert et al., 2016; Müller et al., 2018; Naik et al., 2013; Strode et al., 2015; Yan et al., 2016), which could lead to CO underestimation commonly seen in most global CTMs but have not been fully understood yet (Fisher et al., 2017; Shindell et al., 2006; Stein et al., 2014; Tilmes et al., 2015). To provide insights on the sensitivity of our findings on source contributions to the aforementioned factors, we conduct an ensemble of model simulations with different model configurations and report the range of estimates of the source contributions from these simulations. In addition, we compare these results with four other source contribution approaches to examine the rigor of our findings using CAM-chem. KORUS-AQ is a desirable testbed to evaluate and validate the source contribution analysis from tagged CO tracers in CAM-chem, as there are extensive observations and additional modeling tools used for source contribution analysis in this campaign. Here we compare the ensemble of tagged source contribution results with other analyses from (1) the Weather Research and Forecasting (WRF) inert NO_2 tracers (Grell et al., 2005; Pfister et al., 2017), (2) the FLEXible PARTicle dispersion model (FLEXPART) back trajectory calculations driven by WRF (Stohl et al., 2005; Brioude et al., 2013), (3) volatile organic compounds (VOCs) signatures suggested by the Whole Air Sampling (WAS) group from the University of California, Irvine, and (4) observed CO to CO_2 enhancement ratios.

This paper is organized as follows. We introduce models and observations in Section 2. In section 3, we evaluate the performance of CAM-chem simulations of CO during KORUS-AQ. In section 4, we provide the source contribution analysis using a set of CAM-chem simulations with tagged CO for the KORUS-AQ field campaign. In section 5, results of the source contribution analysis by tagged tracers in CAM-chem are compared with four other approaches. Section 6 concludes the study.

2. Observations and Model Descriptions

2.1. Observations During KORUS-AQ

The KORUS-AQ campaign (1 May to 10 June 2016) provides comprehensive observations from aircraft, ships, and ground sites. Three aircraft (NASA DC-8, NASA B200 King Air, and Hanseo King Air) were involved in the campaign. The NASA Langley B200 King Air was outfitted with only remote sensing instruments, so there were no onboard CO measurements for analysis, while Hanseo King Air flight tracks were usually at a relatively small scale. However, the NASA DC-8 aircraft flights covered Korea and its surrounding waters during KORUS-AQ, sampling the lower and middle troposphere (see Figure 1 and Figure S1 in the supporting information). Thus, we use the measurements from the NASA DC-8 aircraft in this study. We also use the CO measurements from three ground sites involved in the KORUS-AQ campaign and the Measurements Of Pollution In The Troposphere (MOPITT) satellite retrievals. Depending on our analysis, model results are shown at all or part from the six sites presented in Figure 1. The date and time in this paper are based on Korean local time.

2.1.1. Observations of CO

Onboard the DC-8 aircraft, CO concentrations were measured by the DACOM/DLH team (Differential Absorption CO Measurement and Diode Laser Hygrometer from Langley Research Center). The DACOM/DLH team used the in situ diode laser spectrometer system (which measured absorption lines of several species including CO with three tunable diode lasers) to take CO measurements with a time response of 1 s, precision of 0.1 ppbv (or <1%), and accuracy of 2% (https://airbornescience.nasa.gov/instrument/DACOM; Warner et al., 2010). In addition, we use in situ CO measurements available from three KORUS-AQ ground sites, including Taehwa (127.311°E, 37.312°N), Fukue (128.682°E, 32.752°N), and Olympic Park (127.124°E, 37.522°N). Taehwa is managed by the National Institute of Environmental Research and uses the Thermo 48i instrument for CO measurements. Fukue is managed by the Japan Agency for Marine-Earth Science and Technology and uses the Thermo 48C instrument (Kanaya et al., 2016). Olympic Park is managed by Korea Research Institute of Standards and Science and employs a KENTEK CO analyzer. To provide a broader spatial context for this study, we also utilize the MOPITT version 7, multispectral thermal-infrared/near-infrared (TIR/NIR), Level 3 retrievals of daytime CO total column density (Deeter, 2017). Onboard the NASA Terra satellite, these retrievals have a spatial resolution at nadir of about 22 km with satellite overpass time around 10:30 a.m. The retrieval qualities can be surface dependent with the effects of geophysical noise generally stronger over land than over the ocean, especially over mountainous regions (Deeter et al., 2015). In MOPITT version 7, meteorological fields from the Modern-Era Retrospective analysis for Research and Applications, Version 2 (MERRA-2) and Moderate-Resolution Imaging Spectroradiometer Collection 6 cloud mask product (instead of Collection 5) are used for retrieving CO. MOPITT version 7 products show generally smaller retrieval biases and reduced bias variability compared to previous versions (Deeter, 2017). The multispectral TIR/NIR products have larger degrees of freedom for signal and higher sensitivity to CO, especially over land and near the surface, compared to the TIR-only products (Worden et al., 2010). The Level 3 products are produced by averaging on a 1° latitude/longitude grid and are less affected by random retrieval errors compared to level 2 products (Deeter et al., 2017).

2.1.2. Observations of CO_2 and VOCs

In addition to CO measurements, we also use measurements of CO_2 collected aboard the DC-8 aircraft for another source analysis approach. The Atmospheric Vertical Observations of CO_2 in the Earth's Troposphere from Langley Research Center team measured CO_2 with high precision using a modified LI-COR model 6252 nondispersive infrared spectrometer (NDIR). The Atmospheric Vertical Observations of CO_2 in the Earth's Troposphere from Langley Research Center team provided CO_2 concentrations by sensing the difference in light absorption between the continuously flowing sample and reference gases (https://airbornescience.nasa.gov/instrument/AVOCET; Vay et al., 2011). The ratio of emitted CO and CO_2 is a measure of combustion efficiency, since incomplete combustion produces CO. The CO to CO_2

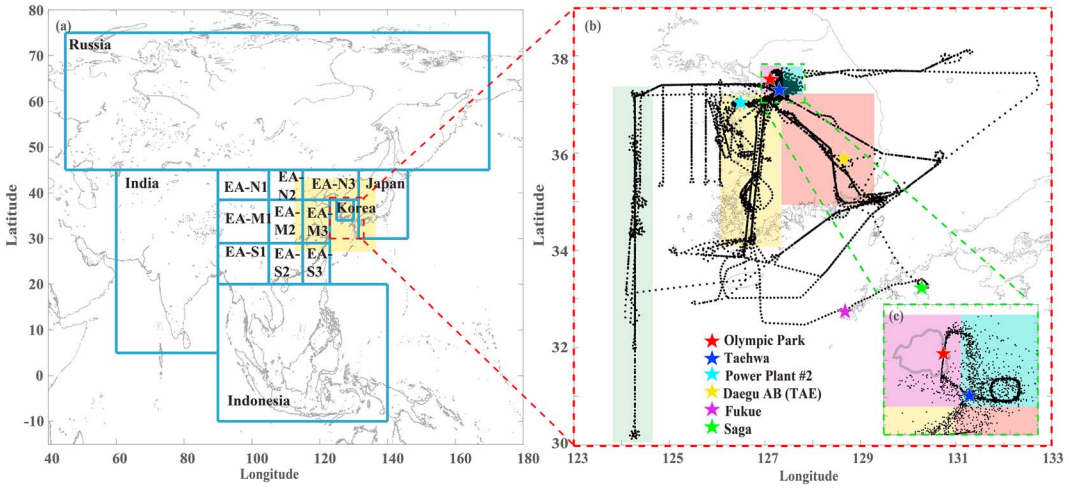

Figure 1. Tagged regions in Community Atmosphere Model with chemistry, domain of FLEXPART 9.1 back trajectory calculations driven by WRF, and DC-8 aircraft flight tracks and locations of ground sites during the Korea United States Air Quality (KORUS-AQ) campaign (1 May to 10 June 2016). (a) Blue rectangles denote 14 tagged source regions in CAM-chem: Korea, Russia, India, Indonesia, Japan, East Asia-North1 (EA-N1), East Asia-North2 (EA-N2), East Asia-North3 (EA-N3), East Asia-Middle1 (EA-M1), East Asia-Middle2 (EA-M2), East Asia-Middle3 (EA-M3), East Asia-South1 (EA-S1), East Asia-South2 (EA-S2), and East Asia-South3 (EA-S3). We assign areas outside these 14 tagged regions as the rest of the world. Yellow-shaded area represents FLEXPART 9.1 back trajectory calculations driven by WRF domain used in this study. (b) DC-8 aircraft flight tracks during KORUS-AQ are shown as dotted lines. The DC-8 aircraft measurements are classified into five groups (Seoul, Taehwa, West Sea, Seoul-Jeju jetway, Seoul-Busan jetway) shown as purple-, blue-, green-, yellow-, and red-shaded areas, respectively. Colored stars represent six ground sites involved in the KORUS-AQ campaign. Also shown in (c) is the zoomed-in version of the green box in panel (b). Gray line denotes political boundary of Seoul.

enhancement ratios (as proxy of emission ratios) have proven to be a useful indicator of anthropogenic combustion efficiency (e.g., Bakwin et al., 1994; Silva et al., 2013; Tang et al., 2018; Turnbull et al., 2011; Wang et al., 2010), despite that the ratios are impacted by various factors including air mass aging and reaction with hydroxyl radical (OH). Besides, we also assume that the potential ocean sink of CO_2 between China and Korea does not significantly influence the source contribution analysis, because of the short transport time of Chinese pollution to the KORUS-AQ domain. We conduct the reduced major axis regression (Smith, 2009) using the DC-8 aircraft CO and CO_2 measurements (every 1 s) to compute the regression slope (dCO/dCO_2) for every minute of each flight data series. The regression slopes (dCO/dCO_2) correspond to the enhancement ratios (Parrish et al., 2002).

VOCs measurements and analysis made by the UC-Irvine WAS group are also used to corroborate our findings derived from the tagged CO simulations. The WAS group (https://espo.nasa.gov/korus-aq/content/WAS_%E2%80%93_UCI) collected whole air samples during the DC-8 aircraft flights and analyzed them at the UC Irvine laboratory using Gas Chromatography for about 90 species of VOCs. The WAS group, as well as previous studies, suggests four China signature VOCs, including CCl_4, CFC-113, CFC-114, and carbonyl sulfide (OCS; Barletta et al., 2009; Blake et al., 1996, 2003, 2004; Palmer et al., 2003; Wang et al., 2006; Xue et al., 2011). Based on the VOC measurements and analyses, the WAS group also find that H-1211 (CF_2ClBr), which was previously used as an indicator of Chinese air masses (Blake et al., 2001, 2003), can no longer be used as an indicator during the KORUS-AQ period. We test the consistency between our source contribution results and their conclusions (see section 5.2).

2.2. Global Model With Tagged CO

2.2.1. Model Description

The Community Earth System Model (CESM) is a global earth system model including the atmosphere, land, ocean, and ice components (Hurrell et al., 2013). CAM-chem is the atmosphere component (ATM) of CESM with chemistry, coupled with the land model (Lamarque et al., 2012). In this study, we use a development version of CESM (cesm2_0_alpha07c). CESM can be configured with various component sets (http://www.cesm.ucar.edu/models/cesm2.0/cesm/compsets.html). Our simulations use the component set of

FCSD, which includes CAM6 physics with chemistry, and the meteorology is relaxed to specified dynamics. Tropospheric and stratospheric chemistry are included, with a volatility basis set secondary organic aerosol scheme and modal aerosols. In our CAM-chem simulations, we use a significantly updated tropospheric chemistry mechanism: Model for OZone and Related chemical Tracers, version T1 (MOZART-T1). MOZART-T1 includes an expansion of the isoprene oxidation scheme, splits lumped aromatics, and terpenes to individual species and has a more detailed representation of organic nitrates (https://www2.acom.ucar.edu/gcm/mozart). The model meteorology (including winds, surface pressure, and temperature) is nudged toward prescribed meteorological fields on their native levels, which is the lower 56 of 72 levels ranging from the surface to ~2 hPa (Bogenschutz et al., 2012, 2018; Liu et al., 2016; Morrison & Gettelman, 2008). In terms of the land component (LND), our configuration uses the Community Land Model Version 5.0. In addition, FCSD also uses the prescribed ocean mode (DOCN%DOM) as well as prescribed sea ice (CICE).

We use three model resolutions, including 0.9° × 1.25° (1-degree; f09_f09), 1.9° × 2.5° (2-degree; f19_f19), and 0.47° × 0.63° (half-degree; f05_g16). For the 1-degree and 2-degree configurations, ATM, LND, OCN, and sea ice model (CICE) use the finite volume grid with the same resolutions of 0.9° × 1.25° and 1.9° × 2.5°, respectively. For the half-degree configuration, ATM and LND use finite volume grid and both have resolutions of 0.47° × 0.63°, while OCN and ICE use the displaced Greenland pole grid of approximately 1° resolution (gx1v6 mask). The displaced Greenland Pole grid is a latitude/longitude grid with the North Pole displaced over Greenland to avoid singularity problems in the OCN and CICE models.

2.2.2. Emissions

We employ three anthropogenic emission inventories with monthly time resolution, including the Hemispheric Transport of Air Pollution (HTAP) version 2 inventory (Janssens-Maenhout et al., 2015), the Community Emissions Data System for Coupled Model Intercomparison Project Phase 6 (CMIP6; Hoesly et al., 2017), and the Comprehensive Regional Emissions Inventory for Atmospheric Transport Experiment (CREATE) embedded in HTAPv2. HTAPv2 provides monthly and annual emissions for CO, SO_2, NO_X, nonmethane volatile organic compounds (NMVOCs), NH_3, PM_{10}, $PM_{2.5}$, black carbon, and organic carbon for the years 2008 and 2010 at a resolution of 0.1° × 0.1°, by compiling regional inventories (e.g., the MIX inventory for Asian anthropogenic emissions; Li et al., 2017). The uncertainties in HTAPv2 CO emissions are 35–70% for the energy and industry sectors and 70–150% for the residential and transportation sectors (Janssens-Maenhout et al., 2015). CMIP6, developed with Community Emissions Data System, provides anthropogenic emissions of CO, CH_4, NH_3, NO_X, SO_2, NMVOCs, and carbonaceous aerosols (black carbon and organic carbon) from 1750 to 2014 at a resolution of 0.5° × 0.5°. The CMIP6 inventory incorporates regional and country-specific inventories and existing energy consumption data sets. Despite the advantageous features in the CMIP6 emission inventory such as usage of updated emission factors and wide span of time, it has some limitations, including disaggregation of key noncombustion sectors and static gridding proxies for residential (and related) emissions. The uncertainties of CMIP6 have not been as well quantified as HTAP (Hoesly et al., 2017). Due to the unavailability of data for year 2016, the HTAP 2010 and CMIP6 2014 emissions are used in this study, with the awareness that using the 2010 or 2014 inventory may not match actual 2016 emissions. CREATE version 1 is a regional inventory developed specifically for the KORUS-AQ campaign (covering China and Korea). We embed CREATE in HTAP because CAM-chem requires a global emission inventory as input.

For biomass burning emissions, we use the Fire INventory from NCAR version 1.5 (FINNv1.5; Wiedinmyer et al., 2011). The FINN inventory is gridded to the CAM-chem resolutions to generate global daily biomass burning emissions for input to CAM-chem. Major uncertainties of FINN come from missed fires (including small fires) and overestimation of the size of detected small fires. However, the two factors tend to cancel each other (Wiedinmyer et al., 2011). Tang and Arellano (2017) suggested that treatment of emission factors in FINN (as well as other biomass burning emission inventories) introduces uncertainties into the emission estimates. Monks et al. (2015) showed that CO emissions in FINN are overestimated over Siberia and Myanmar. We find that biomass burning emissions of CO are much lower than anthropogenic CO emissions over Korea and China but are high in Russia and Indonesia during KORUS-AQ (Figure S2d).

We combine the three anthropogenic emission inventories with the biomass burning emission inventory (hereinafter HTAP+FINN, CREATE+FINN, and CMIP6 + FINN, Figure S2) as input into CAM-chem. Spatial correlations between the combined inventories are 0.80 (HTAP+FINN and CREATE+FINN) and

0.96 (HTAP+FINN and CMIP6 + FINN) over Korea and 0.80 (HTAP+FINN and CREATE+FINN) and 0.68 (HTAP+FINN and CMIP6 + FINN) over East Asia, respectively. Overall, the spatial distributions of total CO emissions from these combined inventories are consistent in the region (Figure S2). The total CO emissions during the KORUS-AQ period (1 May to 10 June) derived from the CREATE+FINN, CMIP6 + FINN, and HTAP +FINN are 3.08×10^{13}, 3.38×10^{13}, and 3.42×10^{13} g, respectively, over East Asia (75–145°E, 15–55°N), while they are 1.89×10^{11}, 2.72×10^{11}, and 3.66×10^{11} g over Korea and its surrounding waters (123–133°E, 30–39°N), respectively.

2.2.3. Meteorological Fields

Our simulations use the meteorological fields generated by the NASA Goddard Global Modeling and Assimilation Office using the operational forecast model Goddard Earth Observing System (GEOS) Model, namely, the GEOS Forward Processing (GEOS-FP) near real time forecast (Molod et al., 2015) and MERRA-2 (Gelaro et al., 2017). MERRA-2 assimilates more observations and includes updates to the GEOS model and analysis scheme (Rienecker et al., 2011). In this study, we prescribed wind fields, surface pressure, and temperature from either GEOS-FP or MERRA-2. The original spatial resolutions of GEOS-FP and MERRA-2 used by CAM-chem are 0.3125° × 0.25° and 0.625° × 0.5°, respectively. They are both regridded to the CAM-chem model resolutions before simulations. Currently, CAM-chem does not run with a nested grid; however, a regional refinement version of CAM-chem is under development based on the CAM model with a spectral element dynamical core (Dennis et al., 2012). Because CO transport is mainly affected by winds (Heald et al., 2003; Liang et al., 2004), we compare CAM-chem wind fields over East Asia when the dynamic is nudge to GEOS-FP or MERRA-2. The differences in the wind patterns averaged over the KORUS-AQ period between the two data sets at 850, 500, and 200 hPa are small and negligible to some extent (Figure S3). We also compare time series of wind speeds at the surface layer from the two data sets over two large Korean cities (Seoul and Busan; Figure S3). In addition, we compare spatial distributions of temperature at the surface layer and surface pressure over East Asia (Figure S4). The surface layer temperature and surface pressure from MERRA-2 are generally consistent with those from GEOS-FP, except in the western and northeastern China, where MERRA-2 tends to have higher temperature and pressure than GEOS-FP (e.g., differences of temperature at the surface layer are typically less than 12%, while differences of surface pressure are typically less than 1%). GEOS-FP and MERRA-2 are the two external meteorological fields currently available to CAM-chem (Lamarque et al., 2012). We recognize that the differences between the two are small, hence may not fully represent uncertainties in the model transport. This is one of the limitations of our study. However, we note that even though the differences between GEOS-FP and MERRA-2 wind, temperature, and pressure fields are small at synoptic scale to mesoscale, they can still be different at mesoscale to local scale, for example, over Seoul and Busan (Figures S3g and S3h). Meteorological fields assimilated by NCAR Data Assimilation Research Testbed (DART) are currently available (Gaubert et al., 2016, 2017). In our further study with CAM-chem, we will also use meteorological fields from DART.

2.2.4. Tagging Approach

We tag CO emitted from different source regions as well as CO produced from chemical processes. Each of these tracers is treated in the model in the same way as the prognostic CO. In particular, the time evolution of the abundance of a specific tracer is calculated in the model from the same continuity equation that includes dynamic (e.g., advection and convection) and physicochemical processes (e.g., dry deposition and CO + OH reaction) but only taking into account specific emissions from a particular region or sector or chemical production. The change in the tracer abundance however does not affect the interactive chemistry in the model (Emmons et al., 2010; Gaubert et al., 2016). We note that the OH fields are calculated online and are not prescribed from previous simulations. Here we tagged CO tracers from 14 source regions shown in Figure 1, which includes Korea, Russia, India, Indonesia, Japan, East Asia-North1 (EA-N1), East Asia-North2 (EA-N2), East Asia-North3 (EA-N3), East Asia-Middle1 (EA-M1), East Asia-Middle2 (EA-M2), East Asia-Middle3 (EA-M3), East Asia-South1 (EA-S1), East Asia-South2 (EA-S2), and East Asia-South3 (EA-S3). We assign areas outside these 14 tagged regions as the rest of the world. In addition to these source regions, we also tagged three megacities (Beijing, Shanghai, and Seoul) for the purpose of matching and comparing with the WRF tracers (see section 2.3). For each source region or megacity, biomass burning and anthropogenic emissions of CO are tagged separately. We note that biomass burning emissions are significantly lower than anthropogenic emissions for the tagged regions during the campaign, so biomass

Table 1
Model Configurations for the 17 CAM-chem Simulations

Simulation name	Resolution	Meteorology	Emissions
C2TK1_G_HF	f09_f09 (0.9′1.25)	GEOS-FP	HTAP (anthro)+FINN (bb)
C2TK1_G_CF	f09_f09 (0.9′1.25)	GEOS-FP	CREATE (anthro)+FINN (bb)
C2TK1_G_CMIP6	f09_f09 (0.9′1.25)	GEOS-FP	CMIP6 (anthro)+FINN (bb)
C2TK1_M_HF	f09_f09 (0.9′1.25)	MERRA-2	HTAP (anthro)+FINN (bb)
C2TK1_M_CF	f09_f09 (0.9′1.25)	MERRA-2	CREATE (anthro)+FINN (bb)
C2TK1_M_CMIP6	f09_f09 (0.9′1.25)	MERRA-2	CMIP6 (anthro)+FINN (bb)
C2TK2_G_HF	f19_f19 (1.9′2.5)	GEOS-FP	HTAP (anthro) + FINN (bb)
C2TK05_G_HF	f05_g16 (0.47′0.63 and gx1v6 mask)	GEOS-FP	HTAP (anthro)+FINN (bb)
Global CO × 2	f09_f09 (0.9′1.25)	GEOS-FP	HTAP (anthro)+FINN (bb), with doubled global anthro CO emissions
EA CO × 2	f09_f09 (0.9′1.25)	GEOS-FP	HTAP (anthro)+FINN (bb), with doubled EA anthro CO emissions
Korea CO × 2	f09_f09 (0.9′1.25)	GEOS-FP	HTAP (anthro)+FINN (bb), with doubled Korea anthro CO emissions
EA-N CO × 2	f09_f09 (0.9′1.25)	GEOS-FP	HTAP (anthro) + FINN (bb), with doubled EA-N anthro CO emissions
EA-M CO × 2	f09_f09 (0.9′1.25)	GEOS-FP	HTAP (anthro)+FINN (bb), with doubled EA-M anthro CO emissions
EA-S CO × 2	f09_f09 (0.9′1.25)	GEOS-FP	HTAP (anthro)+FINN (bb), with doubled EA-S anthro CO emissions
EA & Korea CO × 2	f09_f09 (0.9′1.25)	GEOS-FP	HTAP (anthro)+FINN (bb), with doubled EA and Korea anthro CO emissions
EA & Korea VOC × 2	f09_f09 (0.9′1.25)	GEOS-FP	HTAP (anthro)+FINN (bb), with doubled EA and Korea anthro VOC emissions
EA & Korea CO & VOC × 2	f09_f09 (0.9′1.25)	GEOS-FP	HTAP (anthro)+FINN (bb), with doubled EA and Korea anthro CO and VOC emissions

Note. The simulations are named according to their configurations. Specifically, the naming follows the format of C2TK < resolution>_ < meteorology>_ < emissions inventories>, where "C2TK" represents CESM2 Tags for KORUS-AQ. <Resolution> takes values of "05", "1", "2", corresponding to 0.47° × 0.63°, 0.9° × 1.25°, and 1.9° × 2.5°. "G" and "M" in <meteorology> correspond to GEOS-FP and MERRA-2, respectively. <Emissions inventories> includes "HF" (HTAP+FINN), "CF" (CREATE+FINN), and "CMIP6" (CMIP6+FINN). The nine additional simulations are based on C2TK1_G_HF, with doubled anthropogenic CO and/or VOC emissions over the globe or different regions. CAM-chem = Community Atmosphere Model with chemistry; GEOS-FP = Goddard Earth Observing System Forward Processing; HTAP = Hemispheric Transport of Air Pollution inventory; FINN = Fire INventory from NCAR; CREATE = Comprehensive Regional Emissions Inventory for Atmospheric Transport Experiment; CMIP6 = the Community Emissions Data System for Coupled Model Intercomparison Project Phase 6; MERRA-2 = Modern-Era Retrospective analysis for Research and Applications, Version 2; EA-S = East Asia-South; EA = East Asia; VOC = volatile organic compound.

burning and anthropogenic emissions of CO are analyzed together even though they are tagged separately. Besides direct anthropogenic and biomass burning emissions, we also have tags for global biogenic CO, CO from the ocean, CO from CH_4 oxidation using a yield of 0.75 for CH_4 molecule loss by reaction with OH (Gaubert et al., 2016), and CO from other chemical production besides CH_4. We spin-up the model for 1 year before simulations for the KORUS-AQ period. To compare model results with observations, we linearly interpolate the simulated CO concentrations along the location and time of each observational data. The sensitivity of simulation results to model resolution (see section 3) provides insights on how model resolutions contribute to the representation errors introduced by interpolation.

2.2.5. Model Experiments

To explore the uncertainty of CAM-chem CO simulations, we conducted 17 sets of CAM-chem full chemistry with tagged CO tracer simulations. In particular, eight sensitivity test simulations were carried out with varying spatial resolutions, prescribed meteorological fields, or emission inventories. In addition, we conducted nine sensitivity test simulations based on nine emissions scenarios. That is, we increased (e.g., doubled) magnitude of CO emissions for a particular sector or region consistent with reported uncertainties of the bottom-up emission inventories and top-down estimates to further elucidate the influence of emissions to model underestimation of CO in the region. Table 1 shows the definitions and details of the 17 model experiments for this study.

2.3. Regional Models

2.3.1. WRF

Forecasts of inert tracers were provided by NCAR during KORUS-AQ using WRFv3.3.1 with inert tracers similar to the approach employed in Pfister et al. (2017). The outer WRF domain (115.3–138.7°E, 27.7–46.2°N) covers East Asia with a resolution of 15 km × 15 km, and the inner domain (122.4–133.1°E, 31.6–40.6°N) covers Korea with a resolution of 3 km × 3 km. Meteorological fields from the National Centers for Environmental Prediction Global Forecast System at a resolution of 0.5° were used as the

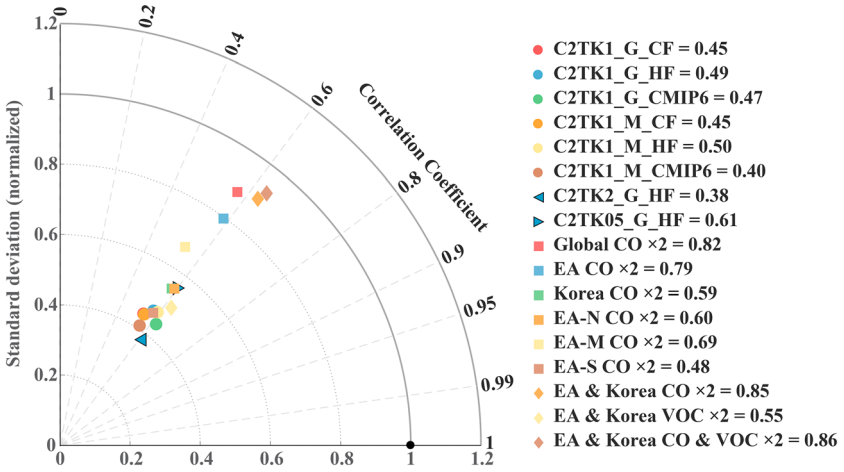

Figure 2. Taylor diagram of CO concentrations during the KORUS-AQ campaign from 17 CAM-chem CO simulations (colored symbols) and airborne CO observations by the DC-8 aircraft (black circle). Circles denote six simulations using the same resolution (0.9° × 1.25°) but two different meteorological (GEOS-FP and MERRA-2) and three different emissions (HTAP+FINN, CREATE+FINN, and CMIP6 + FINN). Triangles denote simulations using two different resolutions (0.47° × 0.63° and 1.9° × 2.5°). Squares and diamonds denote nine simulations by doubling anthropogenic CO and/or VOC emissions over the globe or different regions. See Table 1 for definitions of different CAM-chem simulations. Also shown are Taylor scores (S). KORUS-AQ = Korea United States Air Quality campaign; CAM-chem = Community Atmosphere Model with chemistry; GEOS-FP = Goddard Earth Observing System Forward Processing; MERRA-2 = Modern-Era Retrospective analysis for Research and Applications, Version 2; HTAP = Hemispheric Transport of Air Pollution inventory; FINN = Fire INventory from NCAR; CREATE = Comprehensive Regional Emissions Inventory for Atmospheric Transport Experiment; CMIP6 = the Community Emissions Data System for Coupled Model Intercomparison Project Phase 6.

initial and boundary conditions. The WRF tracers are scaled to NO_2 emissions from CREATE and defined to have a 2-day lifetime for Korean sources and a 4-day lifetime for three selected China regions. More details on model configurations are described in Pfister et al. (2017). In this study, we compare our tagged tracer results from directly emitted CO simulated by CAM-chem (section 2.2) with the WRF inert NO_2 tracers. We note that the CAM-chem CO and WRF NO_2 tracers are very different since the CO tracers in CAM-chem undergo chemical transformation and exhibit a longer lifetime, whereas the NO_2 tracers in WRF are inert with a prescribed lifetime much shorter than CO. We also note that our tagged regions ("Korea," "Beijing," "Shanghai," and "EA-M3") are not exactly equivalent to the counterparts in WRF due to differences in definition and resolution. For these reasons, the comparisons can only be analyzed qualitatively.

2.3.2. FLEXPART

The FLEXible PARTicle dispersion model (FLEXPART) is a Lagrangian transport and particle dispersion model (Stohl et al., 2005), which can be run either forward or backward in time (Seibert & Frank, 2004). FLEXPART can also work with limited-area models such as WRF (Brioude et al., 2013). Here we use FLEXPART 9.1 back trajectory calculations driven by WRF (FLEXPART-WRF) meteorology at 3-km × 3-km horizontal resolution similar to the inner domain described in section 2.3.1. For each DC-8 aircraft observation (every 1 minute along the flight track), back trajectories are calculated following the air mass for 5 days back in time (Stohl et al., 2002). In order to estimate contributions to the observed CO concentrations, we fold the surface sensitivity function calculated by FLEXPART (defined as the sensitivity below 100 m above ground level) with the CO emissions for each region of interest. We assume that CO tracers are inert in the atmosphere and do not account for photochemical loss or production of CO. The FLEXPART-WRF domain is shown in Figure 1a (roughly 115–136°E, 27–43°N). Two of the CAM-chem tags (Korea and EA-M3) are covered entirely by the FLEXPART-WRF domain.

3. Evaluation and Sensitivity Study of CAM-Chem CO Simulations

We first evaluate our CAM-chem simulations of CO by comparing with the DC-8 aircraft measurements supplemented with MOPITT retrievals during KORUS-AQ. A summary of this evaluation is shown in Figures 2,

S5, and S6 and Table S1. We will first focus the discussion of our results on simulations using bottom-up emission inventories followed by our results on simulations using alternative emissions.

Figures S5a–S5c show the mean vertical profiles of the observed CO concentrations and the modeled-observed CO concentration differences. Overall, we find that the simulations with a 1-degree resolution and/or different meteorological fields using bottom-up emission inventories all underestimate CO concentrations across the profile by up to 50 and 130 ppbv above and below 700 hPa, respectively. The use of different meteorological fields (GEOS-FP and MERRA-2) and emission inventories (HTAP+FINN, CREATE +FINN, and CMIP6+FINN) has relatively small effects (differences <20 ppbv) on modeled mean CO profiles (Figure S5b). This is due to the small differences among the meteorological or emission data sets (see section 2.2). However, using 1-degree (0.9° × 1.25°) model resolution, instead of 2-degree (1.9° × 2.5°), improves simulation results by up to ~20 ppbv across most of the levels in the mean vertical profile, particularly below 500 hPa. The use of finer resolution (0.47° × 0.63°) only slightly reduces model biases below 950 hPa yet increases the underestimation above 850 hPa relative to the 1-degree simulation results (Figure S5c), likely due to the enhanced impact of spatiotemporal errors in emissions by using a finer resolution and/or the uncertainty in model vertical transport. Previous studies also suggested that higher spatial resolutions may not improve model simulations (Valari & Menut, 2008; Wild & Prather, 2006; Yu et al., 2016). However, more accurate and quantitative evaluations of the reasons require further investigation (see also discussions below). From these results, we find that the 1-degree simulation performs better than the other two in terms of mean vertical profiles. Nevertheless, simulations with the three resolutions all show large negative biases especially near the surface (~100 ppbv). Lastly, these model simulations with different meteorological fields, emission inventories, and resolutions show similar bias patterns (Figures S5b and S5c). In addition to the mean of model biases, profiles of standard deviation (std) of observed CO from DC-8 aircraft and model biases (dashed lines) are also shown in Figures S5a–S5c. This provides information on the high variability of CO (and model biases) during the KORUS-AQ campaign. As we can expect, overall, the large variability in modeled CO surface concentrations can be attributed to local emission and/or boundary layer mixing uncertainties. An increase in variability around 850 hPa is most likely a result of intermittent advection of CO plumes to Korea.

We present in Figures S6a and S6b the probability density functions (pdfs) of the DC-8 airborne observations and aforementioned eight model simulations to show the domain scale statistics (i.e., data across spatial and temporal domain), which is complementary to Figure S5's overall vertical profile statistics (Figures S5a and S5b). First, the pdf for observed CO exhibits a bimodal distribution peaking at around 100 and 200 ppbv. It is also skewed to the right with a long tail at high CO values. The pdfs of the modeled CO are also bimodal but tend to be centered toward the lower values and more importantly exhibit significant underestimation at higher (>200 ppbv) CO values (Figures S6a and S6b), consistent with the negative biases in mean vertical profiles. Among the three simulations with the same emissions (HTAP+FINN) and meteorological fields (GEOS-FP) but different resolutions, the 1-degree simulation gives a slightly lower normalized mean bias (NMB, −35%) and root-mean-square error (RMSE, 110 ppbv) than the half-degree simulation (−37% and 112 ppbv) and the 2-degree simulation (−38% and 114 ppbv). The 1-degree simulations using HTAP +FINN emissions show the lowest biases (34–35%) and RMSE (108–110 ppbv) among the eight simulations (please see Table S1). On average, all these simulations lead to consistent underestimates of CO by 69–79 ppbv (34–39%), attributed most likely due to persistent underestimation of CO emissions (Bey et al., 2001; Miyazaki et al., 2018; Stein et al., 2014; Streets et al., 2006) and will be elaborated further in the following sections.

Indeed, the above analysis revealed that small changes in meteorological inputs (MERRA-2 and GEOS-FP) to CAM-chem result in slight differences in overall model performance (Figure S5b) This is somewhat expected since GEOS-FP and MERRA-2 produced similar large-scale meteorological patterns in this region despite MERRA-2 being a reanalysis product which ingests more observational constraints than GEOS-FP (Gelaro et al., 2017) (see section 2.2.3). As the DC-8 aircraft CO samples represent more of local to regional pollution, the changes that we see (albeit small) suggest that large-scale (hemispheric to continental) transport errors should play a relatively insignificant role. This is further supported by the model ability in capturing observed plumes and its consistency with results of other source contribution approaches (see section 5). We note, however, that errors in the model representation of boundary layer mixing, diurnal patterns of convection, land-sea breeze, as well as ventilation and uplift processes, cannot be ruled out as local scale to regional scale sources of errors.

Increasing the model resolution (1.9° × 2.5°, 0.9° × 1.25°, and 0.47° × 0.63°) has relatively small effects on overall CO simulations (Figure S5c) relative to DC-8 aircraft CO samples. Specifically, increasing the resolution from 1-degree (1.9° × 2.5°) to 1-degree (0.9° × 1.25°) slightly reduces the mean biases by 3%, whereas increasing the resolution from 1-degree (0.9° × 1.25°) to half-degree (0.47° × 0.63°) slightly increases the mean biases by 2% (Table S1). The better performance of 1-degree is also expected as the domain statistics represent a large-scale rather than local feature, washing away the impact of higher resolution. In addition, the impact of large spatiotemporal errors in emissions is potentially enhanced in higher-resolution simulations leading to relatively large biases. However, improvements in model performance using higher resolution can be evident in the modeled versus observed CO correlations (see Figure 2 and later discussion). Our finding is consistent with Tang et al. (2018) who found that increasing resolution from 16 to 9 km generally produce better CO forecasts in the Copernicus Atmosphere Monitoring Service global prediction system, although in some cases particularly over Seoul and point sources, the 9 km did not show improvements from 16 km. We note, however, that previous studies suggested that increasing model resolution does not necessarily improve model simulations (Valari & Menut, 2008; Wild & Prather, 2006; Yu et al., 2016). Here we use the 1-degree (0.9° × 1.25°) resolution in the subsequent analysis of source contribution as it provides a compromise between performance and computational expediency.

With regard to model chemistry, we compare the modeled OH to measured OH from Airborne Tropospheric Hydrogen Oxides Sensor based on LIF onboard the DC-8 aircraft (Table S2). As described earlier, reaction of CO with OH serves as the main chemical loss pathway for CO (e.g., Gaubert et al., 2016, 2017). Overall, the modeled OH mixing ratios from the aforementioned eight simulations agree with observations. The normalized mean biases and RMSE ranges from −1% to +9% and 0.14 to 0.15 pptv, respectively (Table S2). However, even a small relative overestimation of OH can have a significant impact on the CO loss on one hand and on the chemical production of CO on the other hand. Uncertainties in CO chemical production from oxidation of CH_4 and NMVOC may also contribute to the model underestimation of CO (Stein et al., 2014). The investigation on the model error due to chemistry and oxidants levels will be investigated in future work.

Uncertainties in emission inputs to CAM-chem are likely to play an important role in the underestimation of modeled CO concentrations relative to those collected by the DC-8 aircraft, given that the airborne measurements of CO are made close to the sources. As noted before, Janssens-Maenhout et al. (2015) reported, for example, that uncertainties in HTAP CO emissions are relatively large (i.e., 35–70% for energy and industry sectors and 70–150% for residential and transportation sectors). To investigate how the uncertainties in CO emissions as well as chemical production influence CAM-chem CO results, we conduct nine additional sensitivity test simulations based on the base case configuration with a resolution of 0.9° × 1.25°, GEOS-FP meteorology fields, and HTAP+FINN emissions (hereinafter the C2TK1_G_HF simulation). Correspondingly, nine additional emissions scenarios are considered, where the anthropogenic CO and/or VOC emissions from the globe or major source regions (e.g., EA, Korea, EA-N, EA-M, EA-S; see also Figure 1) are doubled. Even though they still fall in the uncertainty range provided by HTAP, we note that doubled anthropogenic CO and/or VOC emissions over EA and/or Korea are arbitrary and likely to be overestimated (e.g., Jiang et al., 2017; Yin et al., 2015). In addition, doubling the emissions is not expected to improve the model results in the case that source emissions are missing in the inventory. The simulation with doubled global anthropogenic CO emissions is only used as one of the sensitivity test simulations. It does not necessarily indicate that global or regional anthropogenic CO emissions are underestimated by 50%. In fact, the contribution of direct emissions from regions outside of EA and Korea is rather small; therefore, the differences between doubling global anthropogenic CO emissions from doubling only EA and Korean CO anthropogenic emissions reflect impacts of chemical processes. This is supported by the OH simulations of the ensembles (Table S2). The scenario of doubling the global anthropogenic CO emissions (hereinafter Global_CO_ × 2) changes the OH mean bias compared to the base case C2TK1_G_HF from 3% to −8%, while the OH mean bias of the simulation when CO emissions from only EA and Korea are doubled (hereafter EA_&_Korea_CO_ × 2) is ~0%.

In Figures S5d and S5e, we show the improvements in model performance for the nine alternative simulations scenarios. The model biases decrease substantially (slightly) when CO (VOC) emissions are increased, particularly near the surface. Among the nine simulations, the CO vertical profiles from the Global_CO_ × 2 agree the best (mean bias of −6%) with the mean profiles of the DC-8 aircraft

observations, followed by the simulation with doubled anthropogenic CO and VOC emissions in EA and Korea (hereinafter EA_&_Korea_CO_&_VOC_ × 2) with model mean biases of −12% (Table S1). EA_&_Korea_CO_&_VOC_ × 2, however, has the lowest RMSE (87.60 ppbv) and highest correlation among the 17 simulations (0.63). Correlation with the DC-8 aircraft observations is not improved by Global_CO_ × 2 compared to the base case configuration (0.57). In addition, the pdf of the Global_CO_ × 2 simulation misses the peak at higher CO concentrations (~200 ppbv) and is not able to reproduce the bimodal pdf structure of the DC-8 aircraft observations (Figure S6c). This implies that the significantly reduced mean bias by Global_CO_ × 2 is likely to be due to increased background values instead of better representation of CO pattern in the region.

The model performance for all 17 simulations is summarized in Figure 2 as a Taylor diagram (Taylor, 2001). We also estimate the corresponding Taylor scores for these simulations (see Figure 2 and Table S1). These scores provide indications of model skill in representing the amplitude and pattern of observational variability (see equation S1 for the definition of Taylor score). Among the six 1-degree simulations using different meteorological fields and/or emissions, the simulations using HTAP+FINN still have slightly higher Taylor scores than the others, consistent with our previous findings. We find that the Taylor scores increases from 0.38 to 0.49 and further to 0.61 as the model resolution increases from 1.9° × 2.5° to 0.9° × 1.25° and further to 0.47° × 0.63° (Figure 2). This indicates that while increasing resolutions from 0.9° × 1.25° to 0.47° × 0.63° slightly increase model biases (Table S1), the model skill in representing the pattern of observational variability is improved. EA_&_Korea_CO_&_VOC_ × 2 has the highest Taylor score (0.86) among all the 17 simulations, followed by EA_&_Korea_CO_ × 2 (0.85) and Global_CO_ × 2 (0.82), indicating that anthropogenic CO emissions play a more important role than anthropogenic VOC emissions in the region in terms of performance of CAM-chem CO. It is also worth noting that even though doubling anthropogenic CO emissions in Korea do not significantly reduce the model bias compared with the C2TK1_G_HF simulation (Table S1), it increases the representation of the pattern in modeled CO variability with the Taylor score increasing from 0.49 to 0.59. In summary, our results show that simulations using bottom-up emission scenarios are consistently low (bias: −34 to −39%) and poorly perform (skill: Taylor 0.38 to 0.61) than simulations using alternative emissions (bias: −6 to −33%; Taylor skill: 0.48 to 0.86).

We also compare all 17 simulations with MOPITT retrieved CO vertical profiles by interpolating CAM-chem CO onto the MOPITT level 3 grid and pressure levels and further applying the MOPITT averaging kernels to model results to make quantitative comparisons. Figures S5f–S5j show CO vertical profiles from MOPITT averaged over Korea and its surrounding waters (123–133°E, 30–39°N) during the KORUS-AQ period and corresponding differences between observations and CAM-chem simulations. Overall, even without doubling the anthropogenic emissions, the differences between model and MOPITT are relatively small (<40 ppbv), compared to the model biases against airborne observations (Figures S5b–S5e). The bias patterns for different model simulations in comparison with MOPITT are similar to those in comparison with airborne observations. For example, using different meteorological fields and emission inventories has small effects on simulated CO vertical distributions (Figure S5g), with the C2TK1_G_HF simulation performing slightly better than the others. Figure S5h shows that the results using resolutions of 0.9° × 1.25° and 1.9° × 2.5° are very close, with negative biases of <30 ppbv, while the simulation using the resolution of 0.47° × 0.63° gives slightly larger negative biases. Figure S5i and S5j indicate that doubling anthropogenic CO and VOC emissions over East Asia and Korea (EA_&_Korea_CO_&_VOC_ × 2), doubling anthropogenic CO emissions over East Asia and Korea (EA_&_Korea_CO_ × 2), and doubling anthropogenic CO emissions over East Asia (hereafter EA_CO_ × 2) lead to slight (≤6%) overestimates in the lower and middle troposphere, while Global_CO_ × 2 has stronger overestimates (≤20%). This is different from the results of comparisons with airborne observations, where Global_CO_ × 2 agrees best with DC-8 aircraft profiles, which is partially due to differences in sampling time and regions between MOPITT and DC-8 aircraft measurements. Furthermore, the spatial distributions of MOPITT and modeled CO total column density (Figure S7) indicate that all the 17 simulations tend to overestimate in the southern part of East Asia (EA-S; see also Figure 1) and most of the simulations underestimate in the northern part of East Asia (EA-N). Global_CO_ × 2 shows the lowest underestimate in EA-N but the highest overestimate in EA-S (Figure S7). We note that a comprehensive evaluation of MOPITT CO over the region against KORUS-AQ airborne observations requires further study and is beyond the scope of this work.

Overall, the simulations with increased anthropogenic CO and/or VOC emissions result in a substantial model improvement compared with the base case simulation (C2TK1_G_HF) during the KORUS-AQ campaign. This also implies that the underestimated anthropogenic CO emissions as well as chemical production are likely to be the main cause of CO underestimation by CAM-chem during KORUS-AQ in this study. This is consistent with Gaubert et al. (2016) and other data assimilation and inverse modeling studies (Flemming et al., 2017; Jiang et al., 2017; Miyazaki et al., 2017; Yin et al., 2015). We note that although doubling anthropogenic CO emissions may not be the optimized solution, the model improvements obtained by increasing these emissions could still shed light on understanding CO underestimates in global models, particularly considering the large uncertainties in current emission inventories. Here the sensitivity study also implies that more future work needs to be done on refining CO emissions in different source regions.

To emphasize the uncertainties in our source contribution analysis and to take advantage of the ensemble, we provide ranges derived from the top 50% well performed ensemble members (based on Taylor score) for the following source contribution analysis (see sections 4 and 5).

4. Analysis of Source Contributions to Observed CO

In this section, we present analyses of source contribution to CO concentrations collected from DC-8 aircraft and at ground sites and cities during KORUS-AQ. The results are based on the top 50% well performed CAM-chem simulations with CO tags. To this aim, we use the Taylor skill scores presented in section 3 to rank the 17 simulations in terms of model performance (Table S1). We note that the model-observation discrepancies, albeit reduced by adjusting CO and/or VOC emissions, translate into uncertainties in our results, which are estimated source contributions to the CAM-chem modeled CO concentrations that are spatiotemporally collocated with the DC-8 aircraft and ground-based measurements. Nevertheless, CAM-chem tagged CO is still a powerful tool to analyze source contribution for the observations, and the uncertainties in our source contribution analysis are addressed by the range derived from the ensemble.

4.1. Modeled Source Contributions to DC-8 aircraft observed CO

Flight tracks of the DC-8 aircraft during KORUS-AQ and their grouping (Seoul, Taehwa, the West (Yellow) Sea, Seoul-Jeju jetway, and Seoul-Busan jetway) are shown in Figure 1. These five groups are defined based on the land cover below the flight tracks and the sources of pollution following Tang et al. (2018). The Seoul group contains air samples over the metropolitan area of Seoul, while the Taehwa group contains air samples over a forest area near Seoul. Measurements in the West Sea group were designed to capture pollution outflow from China and Korea to the West Sea. Measurements in the Seoul-Jeju jetway and Seoul-Busan jetway groups were both made above the Korean Peninsula. Strong local point sources (such as power plants and industrial regions) are located below the Seoul-Jeju jetway, whereas flights in the Seoul-Busan jetway are designed to capture activities in forest, rural, and Busan urban regions. Figure 3 shows the contributions of different source regions to CO mixing ratios along the DC-8 flight tracks from the top 50% well-performed simulations, including EA & Korea CO & VOC × 2, EA & Korea CO × 2, Global CO × 2, EA CO × 2, EA-M CO × 2, C2TK05_G_HF, EA-N CO × 2, Korea CO × 2, and EA & Korea VOC × 2. The differences between Global_CO_ × 2 and EA_&_Korea_CO_ × 2 are significantly attributed to the CO chemical production besides CH_4. Note that because CH_4 surface mixing ratios are prescribed in CAM-chem, CO production from CH_4 remains similar between the simulations while only CO chemical production from NMVOCs is impacted by doubling anthropogenic CO emissions outside of EA and Korea. This indicates that doubling anthropogenic CO emissions outside of EA and Korea indirectly impact CO background significantly through secondary CO processes. Here uncertainties in chemical processes of CO are reflected coincidentally via increase in CO direct emissions outside of KORUS-AQ domain. Figure 4 shows the spatial distributions of the tagged CO averaged across the KORUS-AQ period. We also provide modeled contributions from different sources for the plumes encountered by the DC-8 aircraft (Figure 5). These plumes were identified by the KORUS-AQ Plume Flagging Team (https://www-air.larc.nasa.gov/cgi-bin/ArcView/korusaq). First, they normalized the DC-8 aircraft CO measurements by median vertical profiles. These normalized CO measurements are then marked as plumes when they are above the respective 98th percentile. In many of these plumes, the modeled contributions from one or two sources are usually dominant and hence regarded as the major source/s for these plumes. However, in some plumes (such as plumes during the 20 May aircraft

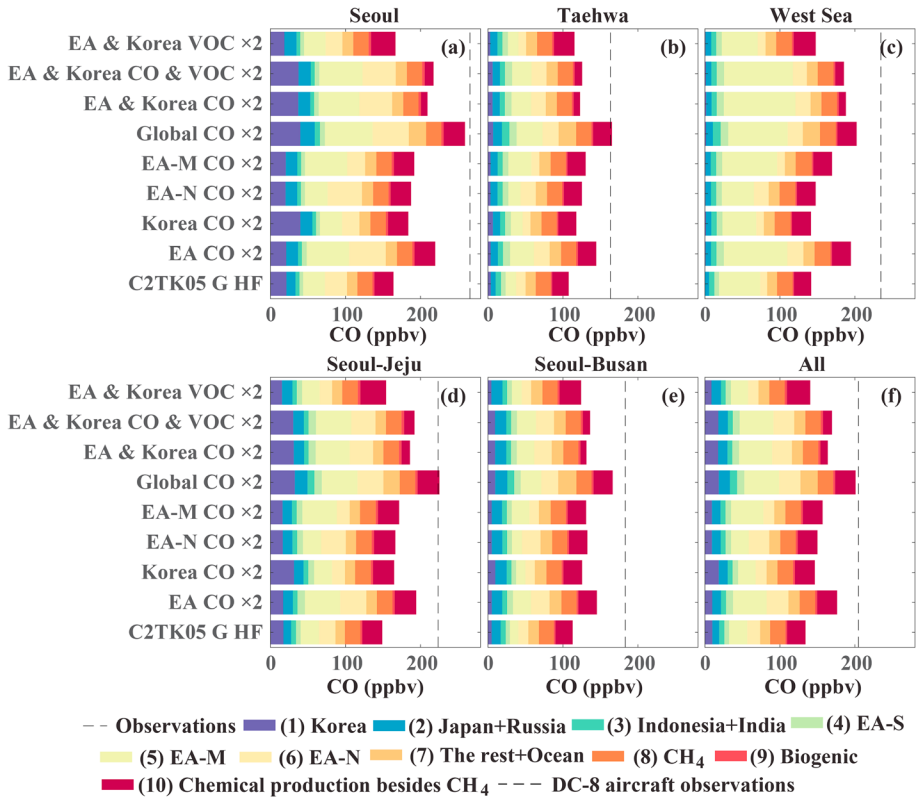

Figure 3. Ensemble of mean estimates of Community Atmosphere Model with chemistry source contributions to CO concentrations along the DC-8 aircraft flight tracks during the Korea United States Air Quality campaign period for all tracks and five track groups defined in Figure 1. Different colors indicate tagged CO sources (see text for details). Dashed lines represent DC-8 aircraft observations.

flight), there is no dominant signature associated with these plumes. Below, we discuss in some detail our key findings which we organized by major source categories.

4.1.1. Contribution of Direct Korean CO Emissions

Throughout the campaign period, direct anthropogenic and biomass burning emissions of CO from Korea vary significantly among the five groups of DC-8 aircraft flights. The contribution of direct Korean CO emissions to modeled CO concentrations over Seoul (10–22%) is the highest among the groups (Figure 3). This is quite expected as Seoul is a megacity and has larger local emissions than its neighboring cities. The Korean emissions also contribute to the modeled CO concentrations over the Seoul-Jeju jetway (9–19%) but only slightly to CO over the Seoul-Busan jetway group (4–8%). This is related to the fact that some strong local point sources (such as power plants and Daesan Chemical Facility) are located in the domain of the Seoul-Jeju jetway (Figure 1). The contribution of Korean CO emissions to CO over Taehwa group (3–6%) is lower than that over Seoul, although Taehwa is near Seoul. CO concentrations observed over Seoul represent CO from urban areas, while over Taehwa CO concentrations are more likely coming from biogenic CO sources over the forest, which may explain the difference between the two groups. We also note that the DC-8 aircraft measurements over Seoul are mostly made below 850 hPa, while more than half of the measurements are made above 850 hPa over Taehwa, which can also contribute to the difference. Over the West Sea, the contribution from direct Korean emissions is very small (~0–1%). This is reasonable since the wind direction on average in this area is from west to east (Figure S3), leading to negligible transport from Korea to the West Sea (although from time to time there are CO outflow albeit near the coast due to land-sea breeze). Moreover, measurements in this group of flights were usually made when Chinese outflow was expected, resulting to rather small Korean contributions to modeled CO. On average, direct Korean CO emissions to modeled CO concentrations only contribute about 6–13% to modeled CO along the DC-8 aircraft flight tracks throughout the campaign period (Table 2).

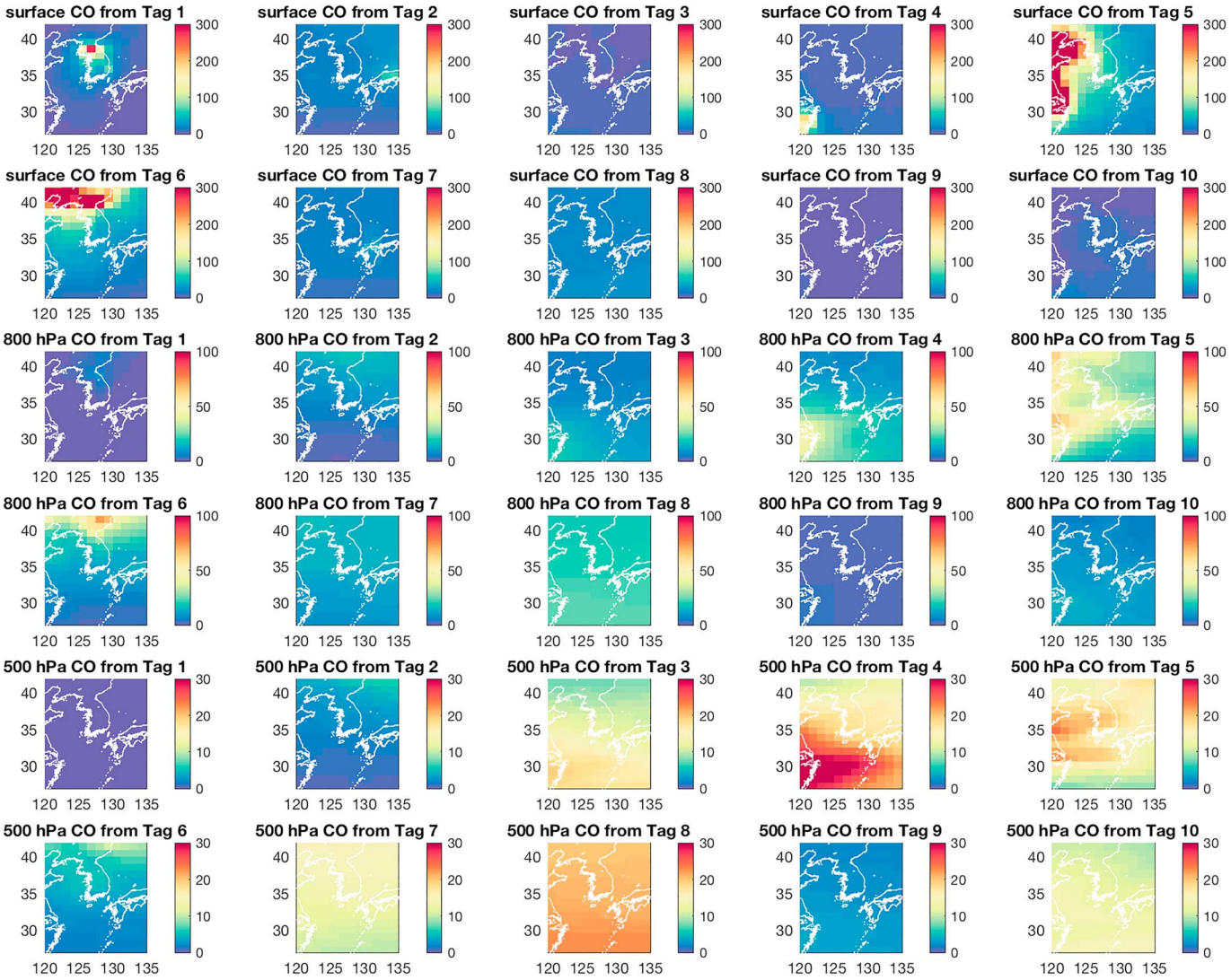

Figure 4. Spatial distributions of the tagged CO (ppbv) averaged across the Korea United States Air Quality campaign period at model surface and 800 and 500 hPa. The results are from the EA_&_Korea_CO_&_VOC_x2 simulation only for demonstration purpose. Tag 1: Korea; Tag 2: Japan+Russia; Tag 3: Indonesia+India; Tag 4: EA-S; Tag 5: EA-M; Tag 6: EA-N; Tag 7: ROW+ocean; Tag 8: CH_4 oxidation; Tag 9: biogenic; Tag 10: chemical production besides CH_4. EA-S = East Asia-South; EA-M = East Asia-Middle; EA-N = East Asia-North; ROW = rest of the world.

We further analyzed this source contribution by separately analyzing airborne measurements below and above 850 hPa to investigate the overall differences between boundary layer and free tropospheric contributions. Here we approximate the boundary layer height to reach on average to about 850 hPa although we recognize that the height varies over time. The results suggest that the Korean contribution to modeled CO along the DC-8 aircraft tracks mainly concentrates in the boundary layer. This is especially the case for the flight tracks over the local sources (Table 2). For example, over Seoul the Korean CO emissions contribute 11–24% and 1–2% below and above 850 hPa, respectively; over Seoul-Jeju jetway, the contributions are 11–25% and ~1%, respectively. Overall, the contribution of Korean CO emissions to modeled total CO is 8–19% below 850 hPa and ~1% above 850 hPa.

The flight on 5 June was designed to sample a number of point sources such as industrial sites, chemical facility, and power plants; thus, the contributions of Korean CO emissions to the DC-8 aircraft observations are higher (11–20%) compared to usual (4–7%; see also Figures 5 and S8). During this flight, the contribution of direct CO emissions from Korea to modeled CO along the tracks is significant, particularly when the flight is close to the surface (~1,000 hPa), as strong local point sources dominate rather than transported CO. We

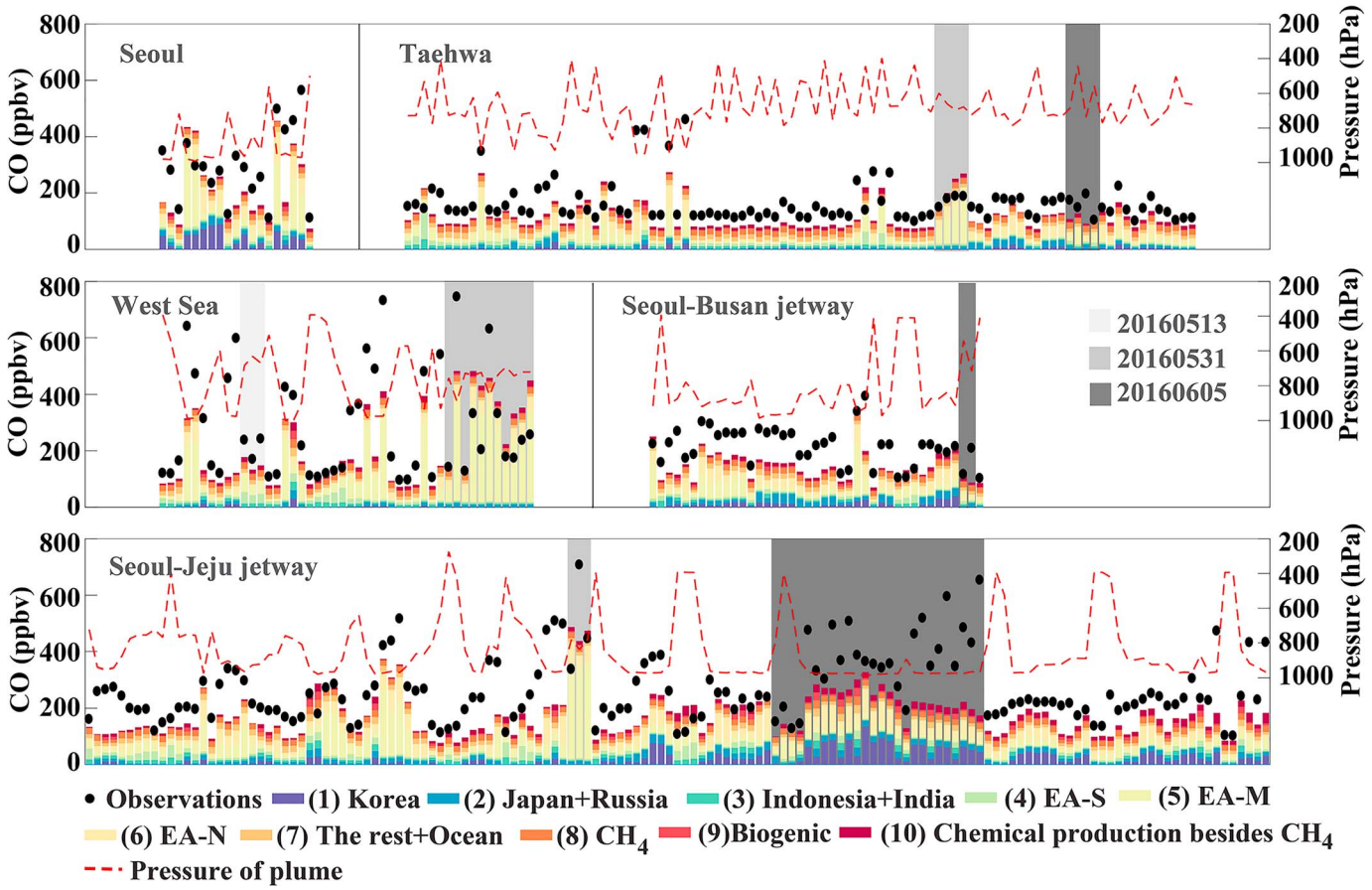

Figure 5. Community Atmosphere Model with chemistry source contributions to all identified CO plumes captured by DC-8 aircraft measurements during the Korea United States Air Quality campaign. The results are from the EA_&_Korea_CO_&_VOC_ × 2 simulation only for demonstration purpose. Different colors indicate tagged CO sources (see text for details). Black dots represent DC-8 aircraft observations. Red dashed lines represent pressures at which the plumes were encountered. Gray shades are used to highlight plumes on three specific days. Note that the *x* axis represents the plume ID.

note that CAM-chem generally captures the plumes throughout the KORUS-AQ period (Figure 5), suggesting that transport is well represented in CAM-chem. However, we note that the model tends to underestimate CO concentrations for the plumes that are associated with strong contributions of Korean CO emissions. This indicates that the CO emissions for these point sources may be underestimated, and/or the relatively coarse resolution (1°) is unable to resolve the local scale emission and dynamic features of these point sources.

4.1.2. Contribution of Direct CO Emissions From East Asia

We divided East Asia (EA) source regions into three subregions, including the northern (EA-N), middle (EA-M), and southern (EA-S) parts as shown in Figure 1. We find that the source contribution of the three subregions has different characteristics. During the measurement period, direct CO emissions from EA-S, EA-M, and EA-N overall contribute ~5%, 16–28%, and 9–18% to modeled total CO along the flight tracks, respectively. Over Seoul, contributions of CO emissions from EA-S, EA-M, and EA-N are about ~3%, 16–29%, and 12–24%, respectively, revealing a much smaller influence from EA-S emissions. Over Taehwa, EA emissions generally contribute less than those over Seoul (Table 2). Over the West Sea, CO concentrations are dominated by CO emissions from EA-M (29–51%), whereas EA-N and EA-S emissions only contribute to 6–13% and 4–5%. Considering that the measurements in this group of flights were usually conducted when Chinese outflow was expected, our result indicates that the East Asian outflow to the West Sea and further to Korea is mainly from the middle part of East Asia (EA-M). We cannot rule out, however, the possibility that EA-N emissions are underestimated and EA-M emissions are overestimated in CAM-chem. Initial results from a separate study on CO Bayesian synthesis inversions, where aggregated tagged CO emissions are optimized using DC-8 aircraft observed CO concentrations, point to this possibility. On the other

Table 2
CAM-chem Simulated Source Contributions to CO Concentrations Along the DC-8 aircraft Flight Tracks During KORUS-AQ

Tagged source	Pressure level	Seoul	Taehwa	West Sea	Seoul-Jeju jetway	Seoul-Busan jetway	All
Korea	All	10–22%	3–6%	0–1%	9–19%	4–8%	6–13%
	Above 850 hPa	1–2%	1–3%	0–0%	1–1%	1–2%	1–1%
	Below 850 hPa	11–24%	6–14%	0–2%	11–25%	5–11%	8–19%
Japan + Russia	All	7–10%	6–8%	4–5%	7–9%	9–12%	7–9%
	Above 850 hPa	4–5%	5–7%	2–3%	4–5%	5–7%	4–5%
	Below 850 hPa	7–10%	9–12%	4–7%	7–10%	12–15%	8–11%
Indonesia + India	All	2–3%	5–7%	4–5%	3–4%	5–6%	4–5%
	Above 850 hPa	5–7%	6–8%	7–9%	7–10%	8–10%	7–9%
	Below 850 hPa	2–3%	3–4%	2–3%	2–3%	3–4%	2–3%
EA-S	All	3–3%	6–8%	4–5%	4–5%	5–6%	5–5%
	Above 850 hPa	5–7%	7–9%	7–10%	10–15%	7–10%	8–11%
	Below 850 hPa	2–3%	3–3%	3–3%	2–3%	3–4%	3–3%
EA-M	All	16–29%	12–24%	29–51%	15–27%	10–19%	16–28%
	Above 850 hPa	18–35%	12–23%	17–37%	14–26%	8–15%	14–26%
	Below 850 hPa	15–29%	14–26%	36–58%	15–27%	11–21%	17–29%
EA-N	All	12–24%	8–16%	6–13%	10–20%	10–19%	9–18%
	Above 850 hPa	7–14%	7–13%	4–8%	5–10%	5–10%	5–10%
	Below 850 hPa	13–26%	13–25%	7–17%	12–23%	12–24%	11–22%
The rest + ocean	All	7–9%	10–14%	8–11%	7–10%	11–15%	9–11%
	Above 850 hPa	9–13%	11–15%	11–15%	10–14%	13–18%	11–15%
	Below 850 hPa	6–8%	8–11%	6–9%	6–8%	9–13%	7–10%
CH_4 oxidation	All	8–12%	12–19%	10–15%	9–14%	12–18%	10–15%
	Above 850 hPa	12–19%	13–20%	14–20%	13–19%	15–22%	14–20%
	Below 850 hPa	7–12%	9–14%	8–13%	8–12%	10–15%	8–13%
Biogenic	All	1–2%	1–2%	1–2%	1–2%	2–2%	1–2%
	Above 850 hPa	1–2%	1–2%	1–2%	1–2%	2–2%	1–2%
	Below 850 hPa	1–2%	1–2%	1–1%	1–2%	1–2%	1–2%
Chemical production besides CH_4	All	4–19%	7–24%	5–20%	6–22%	6–23%	6–22%
	Above 850 hPa	8–24%	8–25%	8–25%	7–25%	10–26%	8–25%
	Below 850 hPa	4–19%	5–21%	3–17%	6–21%	4–21%	5–21%

Note. See text and Figure 1 for definitions of tagged sources and five groups of DC-8 aircraft flight tracks. CAM-chem = Community Atmosphere Model with chemistry; KORUS-AQ = Korea United States Air Quality campaign.

hand, we find that contributions of direct CO emissions from both EA-M and EA-N for the Seoul-Jeju jetway group (15–27% and 10–20%, respectively) are higher than those for the Seoul-Busan jetway group (10–19% and 10–19%, respectively). This is because the Seoul-Jeju jetway is along the west coast of Korea and is closer to EA than the Seoul-Busan jetway.

Along the flight tracks below 850 hPa, direct CO emissions from EA-S, EA-M, and EA-N contribute ~3%, 17–29%, and 11–22% to modeled total CO, respectively. Compared with the results below 850 hPa, the contribution of EA-S emissions is higher above 850 hPa (8–11%). However, the contributions of EA-M (14–26%) and EA-N (5–10%) emissions are lower above 850 hPa than below 850 hPa. This suggests that a large portion of CO emissions from EA-M and EA-N can reach Korea and surrounding areas via transport in the boundary layer, whereas CO emissions from EA-S are likely to be transported to Korea mainly through the free troposphere (particularly during frontal passage periods; see the following analysis). Previous studies (e.g., Liu et al., 2003) also have shown that air pollutants can be lifted from the boundary layer to the free troposphere by fronts in Asian outflows.

In terms of contribution to the plumes, we find that direct CO emissions from EA-M are dominant in the plumes on 31 May (Figures 5 and S9). On 31 May, direct transport of Chinese emissions to the Korean peninsula was expected, so the DC-8 aircraft flew offshore between China and Korea in the morning and then along the Seoul-Jeju jetway in the afternoon. During this flight, CO over the West Sea and along the Seoul-Jeju jetway is dominated by direct emissions from EA-M. These CO source contribution results using CAM-chem tagged tracers support the expected conditions during the science flights. During the two flights in which a frontal passage occurred, the contribution of direct EA-S CO emissions is enhanced. For example, during the 31 May flight, a frontal passage with a cloud band occurred over the Korean peninsula (from the

southwest to the northeast), and the DC-8 aircraft aimed to sample the frontal cloud during the flight. During this measurement period, the EA-S contribution to modeled CO is higher than that during most of the other flights (Figures 5 and S10).

4.1.3. Contribution of Direct CO Emissions From Other Neighboring Regions

Direct CO emissions from Japan, Russia, Indonesia, and India in total only contribute a small proportion to CO mixing ratios along the flight tracks, with contributions of 7–9% from Japan and Russia and 4–5% from Indonesia and India. The contribution of CO from Japan and Russia reaches the maximum (9–12%) for the Seoul-Busan jetway group and the minimum (4–5%) for the West Sea group. For CO from Indonesia and India, the contribution is the highest for the Taehwa group (5–7%) and the lowest for the Seoul group (2–3%). This is likely due to the different altitudes at which measurements were taken by these groups of flights. We further find that the contribution of Japan and Russia is higher below 850 hPa than above 850 hPa, whereas it is the opposite for Indonesia and India (Table 2). This is reasonable, considering that the flight tracks are closer to Japan and Russia than Indonesia and India. As such, it requires strong uplift and subsequent long-range transport of pollution from Indonesia and India to Korea in the free troposphere, consistent with the mesoscale dynamics in this region during this period (Fuelberg et al., 2003; Woo et al., 2003). The differences of the emission response in the vertical between EA-N/EA-M and EA-S/Indonesia/India are also consistent with the results of our doubled emission simulation experiments discussed in section 3.

4.1.4. Contribution From Other Sources

Direct CO emissions from the rest of the world (including ocean) contribute 9–11% to modeled total CO during the entire flight period. Overall, biogenic CO sources have a small contribution (1–2%), whereas CO chemical production plays a relatively important role (10–15% from CH_4 oxidation and 6–22% from chemical production besides CH_4 oxidation) in representing the background CO abundance. One common feature of these sources is that they contribute more to CO in the free troposphere where background CO dominate than in the boundary layer where direct CO emissions from the aforementioned regions dominate. However, we recognize the uncertainties in these estimates as discussed in the previous section (section 3) and elucidated in Figure 3 (Global_CO_ × 2 versus EA_&_Korea_CO_ × 2).

4.2. Source Contribution to Ground Sites and Cities

We also investigated source contributions to surface CO concentrations at six ground sites and to vertical profiles of CO concentrations over Seoul and Busan in Korea during KORUS-AQ. For the ground sites, the patterns of contributions from different sources generally agree with those along the DC-8 aircraft flight tracks (section 4.1). However, direct Korean CO emissions play an obviously more important role at ground sites, especially at sites that are close to large local sources (Figure 6). For example, at the Olympic Park site (located in Seoul), direct CO emissions from Korea contribute more (25–49%) compared to EA-S (~2%), EA-M (11–25%), and EA-N (11–25%) to modeled total CO concentrations, respectively. At Power plant #2 site, the contribution of Korean CO emissions (22–45%) is also higher than those from other source regions (e.g., 1–2% from EA-S, 15–33% from EA-M, and 11–23% from EA-N). Fukue and Saga are two ground sites in Japan. Thus, at these two sites, the Korean contribution is small, whereas the contribution from East Asia and the rest of the world is relatively large. Fukue is a remote site and does not have a strong diurnal cycle, and it captures Asian outflows especially of EA-M and EA-N.

Figure 7 shows the averaged source contributions to CO vertical profiles over Seoul and Busan (in the southeastern South Korea) during KORUS-AQ period (from 1 May 2016 to 9 June 2016). Direct CO emissions from Korea have a much higher contribution to CO concentrations in the two cities near the surface (34–39% for Seoul and 19–20% for Busan) compared to the middle and upper troposphere (<1% for both Seoul and Busan; see also Figures 7a and 7e). We find that due to the larger contribution of Korean CO emissions, the averaged CO concentrations over Seoul are much higher than those over Busan by up to 200 ppbv near the surface. We also show daily averaged profiles of relative contributions on three characteristic days (13 and 31 May and 5 June 2016). As mentioned in section 4.1, a frontal passage occurred on 13 May. On this day, the contribution of direct Korean CO emissions is lower than usual for both Seoul and Busan, whereas a higher contribution from EA emissions is seen, particularly at 800–900 hPa (Figures 7b and 7f). Similar features are also seen on 26 May (another day with a frontal passage; see Figures S11 and S12). On 31 May, direct China outflow was expected. During this period, the contribution of direct CO emissions from EA is much higher than usual,

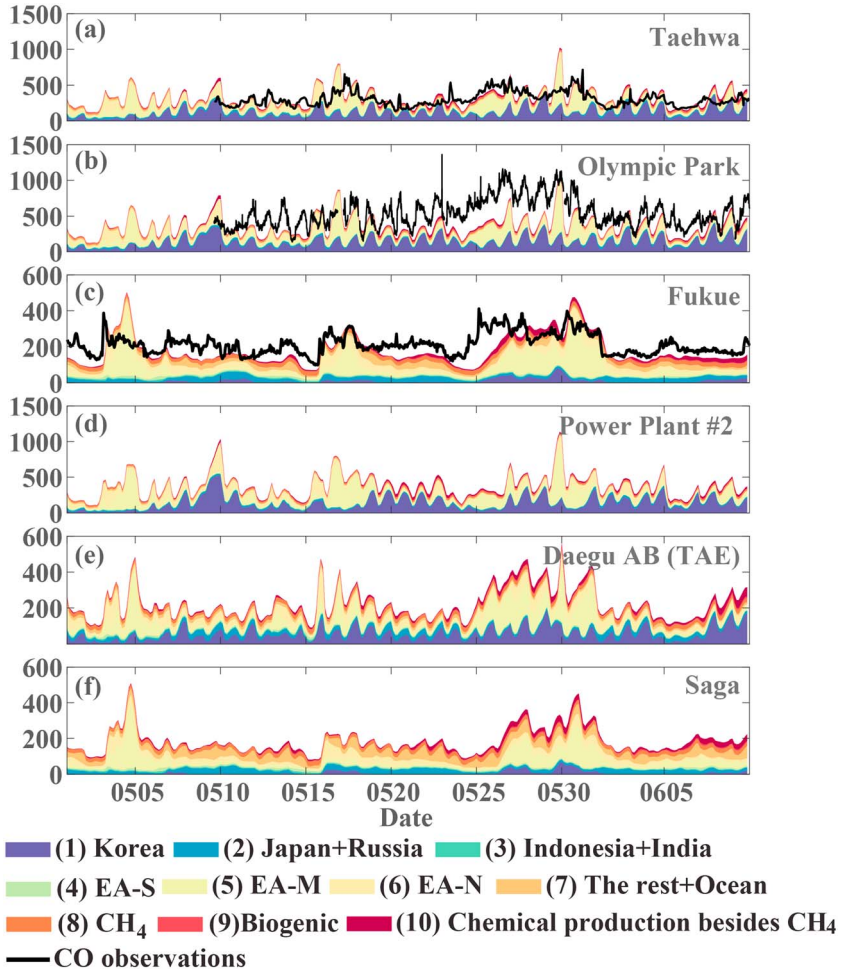

Figure 6. (a–f) Time series of Community Atmosphere Model with chemistry source contributions to CO concentrations at the six ground sites during the Korea United States Air Quality campaign. The results are from the EA_&_Korea_CO_&_VOC_ × 2 simulation only for demonstration purpose. Model results are interpolated to the station locations. Colored areas indicate tagged CO sources (see text for details). Black lines represent corresponding in-situ observations.

especially in the middle troposphere (Figures 7c and 7g). The EA impact is also strong near the surface over Seoul, which is not seen over Busan. On 5 June Chinese emissions were expected to have a smaller impact. Over Seoul and Busan, the CO vertical profiles on this day are similar to those averaged over the KORUS-AQ period. It is worth noticing that, on this day, contributions of Japan and Russia to CO in Seoul are higher than usual because of the prevailing winds.

5. Comparisons With Other Approaches to Source Contributions

In this section, we compare the source contribution results from the CAM-chem tagged CO (derived from EA & Korea CO & VOC × 2 as it is the best performed simulation, unless stated otherwise) with those from the analysis of FLEXPART-WRF back trajectory, WRF-Chem NO_2 tracer, China signature VOCs, and CO to CO_2 enhancement ratios. All the source contribution results from different methods discussed in this section are referred to as contributions of CO emitted from different source regions to modeled total CO along the DC-8 aircraft flight tracks during KORUS-AQ, unless stated otherwise.

5.1. Comparisons With FLEXPART-WRF Back Trajectory and WRF Inert Tracer Analysis

Figure 8 shows the contributions from Korea and EA-M3 CO emissions to CO concentrations along the DC-8 aircraft flight tracks simulated by FLEXPART-WRF and CAM-chem. These are the two source regions

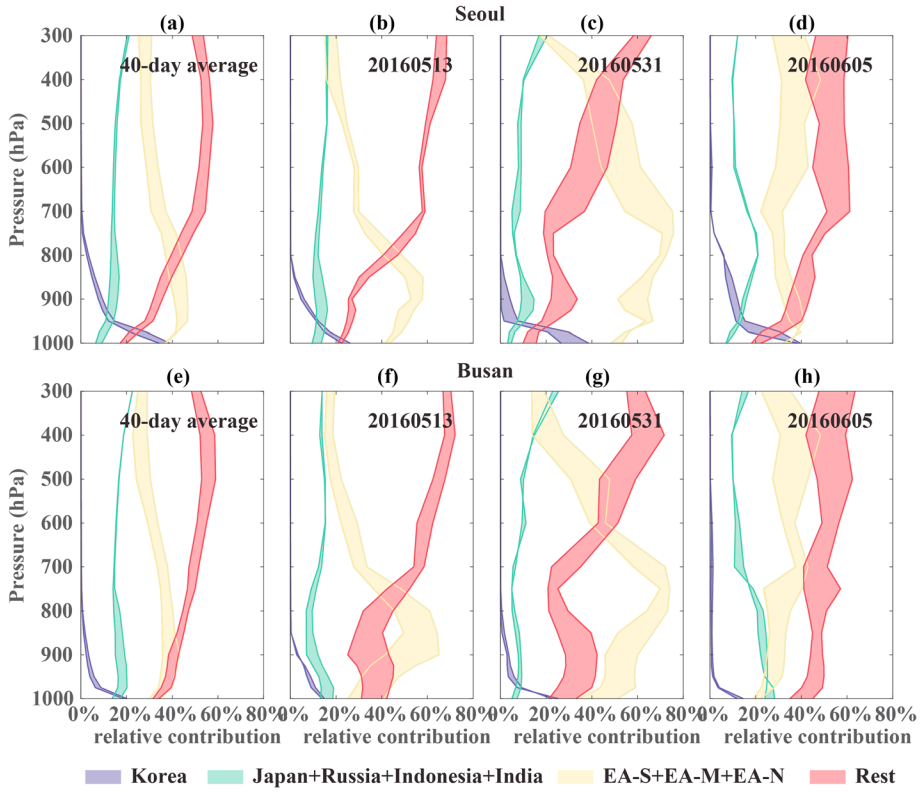

Figure 7. Community Atmosphere Model with chemistry source contributions to CO concentrations at different altitudes over Seoul and Busan during the Korea United States Air Quality campaign for (a, e) 40-day averaged profiles and (b–d, f–h) daily averages of 3 days (20160513, 20160531, and 20160605). The shaded area corresponds to the range of estimates from top 50% of Taylor scores across the ensemble of simulations.

(Korea and EA-M3) that overlapped between the two models. The correlations between the results from FLEXPART-WRF and CAM-chem are 0.77 and 0.56 for the source regions of Korea and EA-M3, respectively. Both FLEXPART-WRF back trajectory and WRF inert tracer analysis are compared to C2TK_G_HF so that they will have same emissions. Although CAM-chem has a coarser resolution than FLEXPART-WRF, the results from the two approaches agree reasonably well. Note that in this comparison, the CAM-chem simulation uses the same CO emissions (HTAP+FINN) as the FLEXPART-WRF back trajectory simulation for consistency.

We also qualitatively compare our CAM-chem results with the WRF inert tracer forecasts during the KORUS-AQ campaign (Figure S13). For contributions from Korean anthropogenic CO emissions along the DC-8 aircraft flight tracks, the correlation between the WRF inert tracer result and CAM-chem tagged CO result is 0.69. This correlation is higher than those for contributions from China anthropogenic source regions (0.47 for Beijing, 0.21 for Shanghai, and 0.49 for Shandong). Because CO in CAM-chem has a longer lifetime than the WRF inert tracer, the higher correlation for tracer contributions from Korean emissions and lower correlations for contributions from Chinese emissions indicate that the WRF inert tracer may be removed more quickly during transport. Therefore, even though East Asia contributes significantly to CO over Korea and surrounding areas during KORUS-AQ, it is possible that its contribution for short-lived species (such as NO_2) is not as significant.

5.2. Comparisons With Analysis of Signature VOCs

Figure 9 shows observations of five anthropogenic VOCs (CCl_4, CFC-113, CFC-114, OCS, and H-1211) that are indicators of pollution from China along the flight tracks during KORUS-AQ and the corresponding CAM-chem simulated CO, including directly emitted CO from Korea, EA, and other regions. We find that CO from direct EA emissions has relatively high correlations with the four suggested China signature

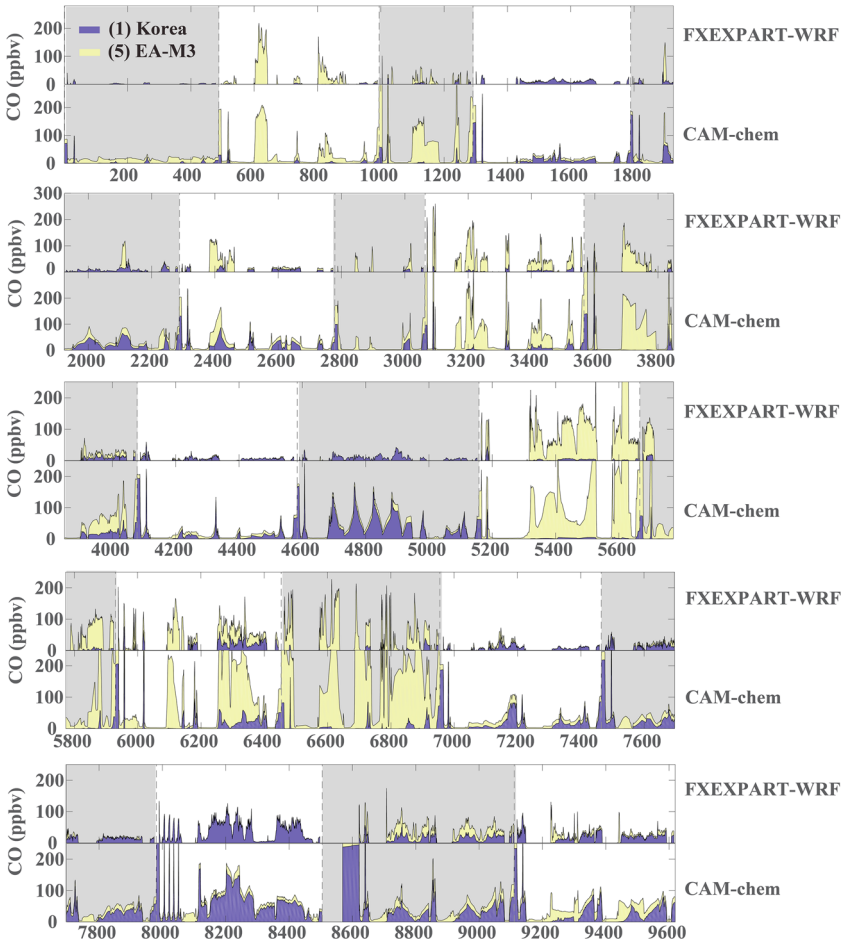

Figure 8. Contributions from Korea (blue) and EA-M3 (yellow) direct CO emissions to CO concentrations along the DC-8 aircraft flight tracks derived from FLEXPART-WRF back trajectories (upper part of each panel) and CAM-chem (lower part of each panel) during the Korea United States Air Quality campaign. The time series are separated into five panels. FLEXPART-WRF = FLEXPART 9.1 back trajectory calculations driven by WRF; CAM-chem = Community Atmosphere Model with chemistry.

VOCs (0.53 for CCl_4, 0.30 for CFC-113, 0.25 for CFC-114, and 0.58 for OCS), which are all statistically significant. However, the correlations for CO directly emitted from Korea (0.01–0.13) and other regions (−0.04–0.11) are much smaller. In addition, the correlation of OCS with CO from direct EA emissions (0.58) is the highest among the four China signature VOCs, while its correlations with CO emitted from Korea (0.01) are the lowest. This implies that OCS could potentially be a more effective indicator of air from China than the other anthropogenic VOC tracers (Qin, 2007). We also show relationships between H-1211 and CO tracers from different sources, which have very weak correlations (r = 0.19 and 0.31 for EA and Korea, respectively). This agrees with the conclusion from the WAS group that H-1211 is no longer a valid China signature VOC during the KORUS-AQ campaign (section 2.1.2).

Given the large area and potential heterogeneity over EA, we further analyzed the relationships between the five VOCs and CO from nine tagged EA subregions and the results are given in Table 3). EA-N1, EA-N2, EA-M1, EA-M2, EA-S1, EA-S2, and EA-S3 do not have strong correlations ($r \leq 0.3$) with the four China signature VOCs (CCl_4, CFC-113, CFC-114, and OCS), whereas EA-M3 has the highest correlation. Correlations of OCS and CCl_4 with CO from EA-N3 (0.24 and 0.30, respectively) are much lower than those with EA-M3 (0.60 and 0.55, respectively), whereas correlations between CFCs and CO from EA-N3 are similar to that for EA-M3 (0.2–0.3). For H-1211 and tagged CO, however, the correlation for EA-N3 (0.20) is higher than that for EA-M3 (0.18). The differences among the nine EA subregions in terms of their relationships with the five VOCs are related with the fact that contributions of CO from some EA regions (such as EA-N1, EA-M1, and

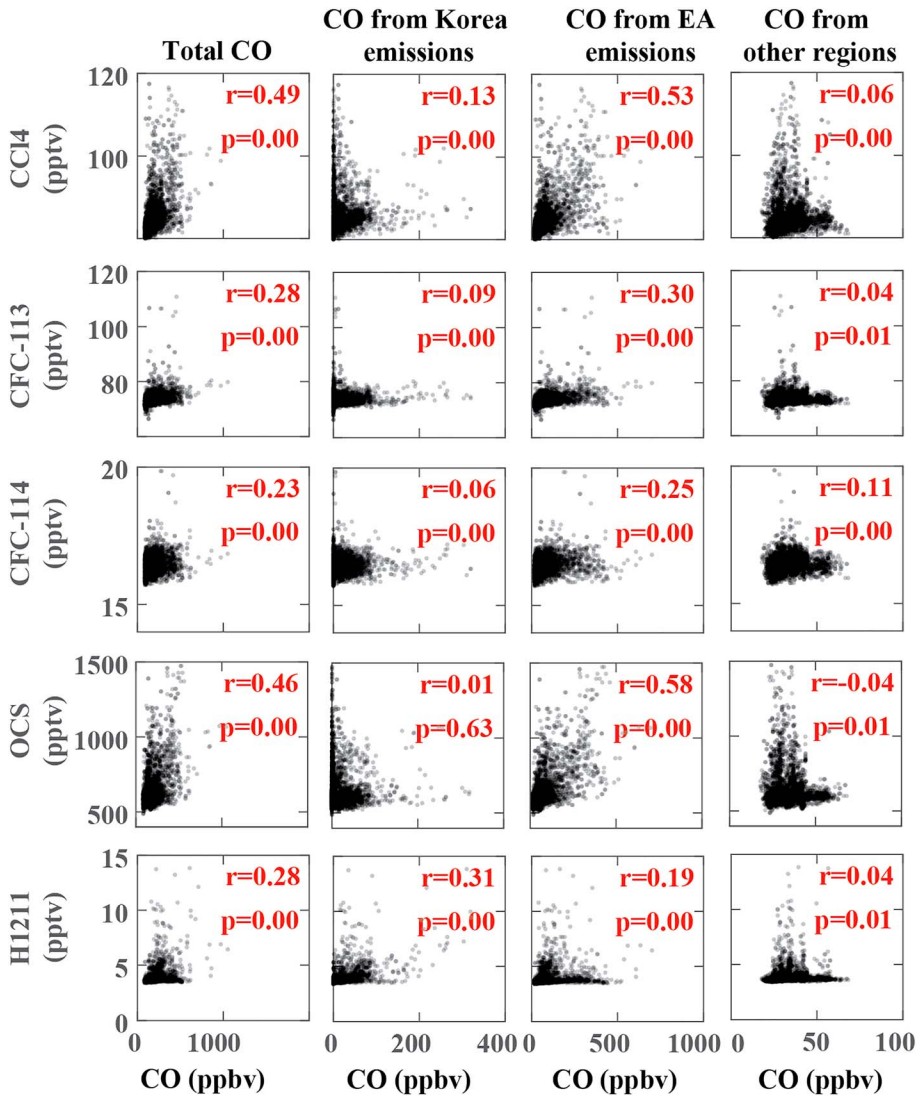

Figure 9. Relationships between CO concentrations contributed from different source regions derived from Community Atmosphere Model with chemistry (EA_&_Korea_CO_&_VOC_ × 2) and volatile organic compound measurements provided by the Whole Air Sampling group along the DC-8 aircraft flight tracks during the Korea United States Air Quality campaign. Correlation coefficients (r) and p values (p) are also shown as red.

EA-S1) are smaller than others (such as EA-N3 and EA-M3). However, it could also be a potential signal of the heterogeneity in anthropogenic VOC emissions over EA.

5.3. Comparisons With Analysis of CO to CO_2 Enhancement Ratios

Previous studies found that dCO/dCO_2 (i.e., CO to CO_2 enhancement ratio; see section 2.1 for definition) are significantly higher for China than Korea, since Korea tends to have overall higher combustion efficiency than China (Silva et al., 2013; Tang et al., 2018; Turnbull et al., 2011; Wang et al., 2010). Thus, a higher dCO/dCO_2 should correspond to a larger China contribution. We compare the dCO/dCO_2 derived from DC-8 aircraft measurements and the corresponding source contributions to CO derived from CAM-chem. Compared with the mean condition (averaged throughout the measurement period), Korean contribution increases from 6–13% to 10–22% over the Seoul group (Table S3), with the corresponding dCO/dCO_2 decreasing from 15.6 to 11.8 ppbv/ppmv. On the other hand, over the West Sea, the contribution from EA increases from 31–49% to 44–67% (Table S3), with the corresponding dCO/dCO_2 increasing from 15.6 to 21.8 ppbv/ppmv. This difference in dCO/dCO_2 indicates that Korea has overall higher combustion

Table 3
Correlations Between CO Concentrations Contributed From Nine East Asia Source Regions Derived From CAM-Chem and VOCs Measured by the WAS Group Along the DC-8 aircraft Flight Tracks During KORUS-AQ

Measured VOC	EA-N1	EA-N2	EA-N3	EA-M1	EA-M2	EA-M3	EA-S1	EA-S2	EA-S3
CCl_4	−0.09	0.18	0.30	−0.14	0.15	0.55	−0.17	−0.08	−0.03
CFC-113	−0.06	0.10	0.17	−0.08	0.08	0.32	−0.09	−0.03	0.01
CFC-114	−0.06	0.06	0.21	−0.04	0.01	0.23	−0.04	0.02	0.04
OCS	0.00	0.30	0.24	−0.07	0.25	0.60	−0.10	−0.05	−0.02
H-1211	−0.08	0.03	0.20	−0.09	0.01	0.18	−0.10	−0.07	−0.06

Note. Shaded cells indicate that the corresponding correlations are not significant (α=0.05). CAM-chem = Community Atmosphere Model with chemistry; VOC = volatile organic compound; WAS = Whole Air Sampling; KORUS-AQ = Korea United States Air Quality campaign; EA-N = East Asia-North.

efficiency than China. Albeit limited in scope, this is qualitatively consistent with our previous findings for Copernicus Atmosphere Monitoring Service CO and CO_2 forecast and analysis products (Tang et al., 2018) and corroborates our new findings of source contributions to this region from CAM-chem tagged CO tracers.

6. Summary and Conclusions

In this study, we investigated CO source contributions for the KORUS-AQ campaign using CAM-chem tagged tracers. We first conducted a set of model sensitivity test simulations by varying emissions, meteorology, and resolution and comprehensively evaluated these CO simulations by comparing with DC-8 aircraft measurements and MOPITT retrievals. We then conducted source contribution analysis for the KORUS-AQ airborne and ground measurements by tagging CO tracers emitted from different source regions and chemical processes in CAM-chem simulations. To further assess the robustness of our analyses of source contributions, we compared the CAM-chem results with the results from four other approaches to source contributions (FLEXPART-WRF back trajectory, WRF inert NO_2 tracer, China signature VOCs, and dCO/dCO_2).

We found that CAM-chem simulations with different spatial resolutions (0.9° × 1.25°, 1.9° × 2.5°, and 0.47° × 0.63°), anthropogenic CO emissions (HTAP, CREATE, and CMIP6), and/or meteorological fields (GEOS-FP and MERRA-2) produce similar bias patterns and systematically underestimate CO vertical profiles by 30–40% (normalized mean bias) during the KORUS-AQ campaign, compared with DC-8 aircraft measurements. We further analyzed the potential sources (transport, emission, resolution, and chemistry) of this underestimation and suggested that chemically produced CO may contribute to the underestimation in CO background in this region. We conducted nine additional sensitivity test simulations by varying anthropogenic CO emissions based on the base case simulation (C2TK1_G_HF), which used GEOS-FP meteorology fields, HTAP+FINN emissions, and the resolution of 0.9° × 1.25°. We emphasize that there are limitations for this approach. We note that doubling anthropogenic CO and/or VOC emissions may not be the optimized solution, and more future work is needed to refine CO emissions and chemistry processes in different source regions. Further studies on the isoprene oxidation and on explaining the biases in the modeled OH values also need to be done. We are also using smooth and prescribed CH_4 fields that may not explain local industrial and oil and gas point sources.

In these nine additional sensitivity test simulations, the anthropogenic CO and/or VOC emissions from the globe or a specific source region (i.e., EA, Korea, EA-N, EA-M, and EA-S) were doubled. We find that simulations using bottom-up emission inventories (HTAP, CREATE, and CMIP6) are consistently low (bias: −34 to −39%) and perform more poorly (Taylor skill: 0.38 to 0.61) than simulations using alternative emissions (bias: −6 to −33%; Taylor skill: 0.48 to 0.86), particularly for simulations with doubled East Asian and Korean anthropogenic CO and VOC emissions, suggesting underestimation in modeled background CO (Global_CO_x2) and bottom-up emissions (EA_&_Korea_CO_&_VOC_x2) in the region. We further compared all the aforementioned model simulations with MOPITT CO retrievals over East Asia during the KORUS-AQ period. The differences in CO vertical profiles between model simulations and MOPITT over Korea and its surrounding areas are much smaller, relative to the model biases against DC-8 aircraft

airborne observations. EA_&_Korea_CO_&_VOC_ × 2 also agrees better with MOPITT compared to Global CO × 2. We also found that all the model simulations tend to overestimate (underestimate) CO total column density in the southern (northern) part of East Asia. We note that a systematic evaluation of MOPITT CO over the region using the KORUS-AQ airborne observations requires further work and is beyond the scope of this work.

To emphasize the uncertainties in our source contribution analysis and to take advantage of the ensemble of model simulations, we provide ranges derived from the top 50% performed ensemble members (based on Taylor score) for our source contribution analysis. We elucidate the contributions of different tagged emissions to CO concentrations along DC-8 aircraft flight tracks and across several ground sites.

The results of CAM-chem tagged CO simulations showed that direct Korean CO emissions overall contribute about 6–13% to modeled total CO concentrations throughout the DC-8 aircraft flight period. The Korean contribution is higher for the Seoul (10–22%) and Seoul-Jeju jetway (9–19%) groups of flight tracks due to the proximity to strong local emissions but much lower for the West Sea group (≤1%) due to the prevailing winds. The contribution of CO from direct Korean emissions to the DC-8 aircraft measurements is larger within the boundary layer (below 850 hPa; 8–19%) than free troposphere (above 850 hPa; ~1%). Contributions of direct CO emissions from Japan, Russia, Indonesia, and India together account for a smaller proportion (10–13%). The contributions of direct CO emissions from different parts of East Asia (EA-S, EA-M, and EA-S) show very different characteristics, with the largest and smallest overall contribution from EA-M (16–28%) and EA-S (~5%), respectively. We found that the contribution from EA-S CO emissions is higher in the free troposphere (8–11%) than in the boundary layer (~3%), while it is the opposite for contribution from EA-M (17–29% in the boundary layer and 14–26% in free troposphere) and EA-N (11–22% in the boundary layer and 5–10% in free troposphere) emissions. In particular, for the West Sea group of DC-8 aircraft flights when Chinese outflow was expected, the contribution of CO emissions from EA-M is evidently larger (29–51%) than average, suggesting that the West Sea region is mainly impacted by the EA-M outflow. Other sources, including direct CO emissions from the rest of the world, biogenic CO, and CO chemical production, generally contribute more in the free troposphere (40–58%) than in the boundary layer (24–44%).

We also analyzed source contributions to the plumes encountered by the DC-8 aircraft. The results are consistent with the source contribution analysis for the general airborne measurements. During the frontal passage days, contribution of EA-S CO emissions to the plumes is enhanced (11–16% to plumes captured on 13 May) compared to the average (6–8%). During the China outflow days, the plumes are dominated by EA-M CO emissions (44–64% to plumes captured on 31 May). For the plumes expected to be dominated by Korea local emissions, the contribution of Korean CO emissions (11–20% to plumes captured on 5 June) is evidently higher than usual (4–7%). Further source contribution analyses for six ground sites and two cities during KORUS-AQ indicated that the results generally agree with those for the airborne measurements, except that direct Korean CO emissions play an obviously more important role, especially at sites close to large local sources.

To further evaluate the robustness of the source contribution results by CAM-chem tagged CO, we compared the CAM-chem results with those from four other approaches to source contributions (FLEXPART-WRF back trajectories, WRF inert NO_2 tracers, China signature VOCs, and dCO/dCO_2). The overall source contribution results from CAM-chem and FLEXPART-WRF simulations agree reasonably well. The correlation between CAM-chem CO tracers with WRF inert NO_2 tracers is higher for emissions from Korea (0.7) than from China (<0.5), which suggests a smaller contribution of Chinese emissions to short-lived air pollutants transported to Korea, relative to long-lived species. Further comparisons with four China signature VOCs (CCl_4, CFC-113, CFC-114, and OCS) showed that modeled CO from direct EA emissions has higher correlations with the China signature VOCs, compared to CO from elsewhere. The results also suggested that OCS could potentially be a more effective indicator of China outflows than the other three signature VOCs, while H-1211 is no longer a valid China signature VOC. Moreover, the different relationships between CO from EA subregions and different China signature VOCs might be a potential signal of the inhomogeneity in VOC emissions over EA. Finally, we found consistent results from CAM-chem tagged tracers and dCO/dCO_2 analysis, which shows that a higher-than-usual contribution of Korean CO emissions corresponds to a lower-than-usual dCO/dCO_2, with the opposite relationship for China. In summary, the source contribution results from CAM-chem tagged CO tracers are reasonably consistent with those from the other four methods.

We note that the CAM-chem CO tagged tracers as well as the other four approaches have advantages and limitations. The tagging method is particularly appropriate for tracers associated with complicated atmospheric processes (e.g., chemistry and deposition), which explicitly accounts for nonlinearity in the sensitivity to changes in emissions. Besides, CAM-chem has a global coverage and represents CO from global emissions, chemistry, and other sources such as biogenic production, but its spatial resolution is not high enough to resolve some local features. On the contrary, FLEXPART-WRF back trajectories and WRF-Tracer used in this study have higher resolutions but cover a much smaller domain and do not include chemistry. VOCs can be reliable pollution tracers, but using VOCs to analyze sources of air is strongly dependent on a priori knowledge. For example, H-1211 was often used as a China signature VOC previously, but during KORUS-AQ it has been found to be no longer a useful indicator for Chinese plumes. The dCO/dCO_2 regression ratio may contain valuable information on combustion efficiency, but a careful analysis along with other supporting data sets and tools (such as radiocarbon and tagged fossil fuel CO_2 tracers) is necessary for a more rigorous interpretation, since this approach can be affected by other confounding factors such as air mass aging and chemical reactions. More quantitative and comprehensive evaluations and comparisons of different source contribution methods are needed in future work. We also note that this study is conducted for the time period of the KORUS-AQ experiment (May–June 2016) and does not necessarily represent the source contributions throughout the year.

Acknowledgments
We thank the KORUS-AQ team for observational data (including the WAS group from UCI for VOC data, the DACOM/DLH team for CO data, the AVOCET team for CO_2 data, Dr. W. Brune and team for the ATHOS measurements, and Dr. J. Hair and the DIAL team for the ozone data). We also thank the CESM and CAM-chem team for technical support. CESM is sponsored by the National Science Foundation (NSF) and the U.S. Department of Energy (DOE). Administration of the CESM is maintained by the Climate and Global Dynamics Division (CGD) at the National Center for Atmospheric Research (NCAR). We thank MOPITT teams for satellite retrievals of CO. The NCAR MOPITT project is supported by the National Aeronautics and Space Administration (NASA) Earth Observing System (EOS) Program. The authors thank the anonymous reviewers for their constructive comments and suggestions. W. Tang thanks the NCAR Advanced Study Program's Graduate Visitor Program. C. He is supported by the NCAR Advanced Study Program Postdoctoral Fellowship. The authors thank Dr. Jean-Francois Lamarque and Dr. Helen Worden for helpful discussions. Yugo Kanaya was supported by the Environment Research and Technology Development Fund (2-1505 and 2-1803) of the Ministry of the Environment, Japan. Computing resources were provided by the Climate Simulation Laboratory at NCAR's Computational and Information Systems Laboratory (CISL), sponsored by the National Science Foundation and other agencies. We would like to acknowledge high-performance computing support from Cheyenne (doi:10.5065/D6RX99HX) provided by NCAR's Computational and Information Systems Laboratory, sponsored by the National Science Foundation. NCAR is sponsored by the National Science Foundation. This work is supported by NASA grants NNX16AD96G, NNX16AE16G, and NNX17AG39G. Observational data, modeling results of WRF, FLEXPART-ERF during KORUS-AQ, are available at https://www-air.larc.nasa.gov/cgi-bin/ArcView/korusaq. MOPITT data are available at https://www2.acom.ucar.edu/mopitt. CAM-chem modeling results are available at https://github.com/EarthSciData/Modeloutput.git.

References

Al-Saadi, Jassim, Gregory Carmichael, James Crawford, Louisa Emmons, Saewung Kim, Chang-Keun Song, et al. (2014). KORUS-AQ: An international cooperative air quality field study in Korea, the KORUS-AQ white paper, 2014 (https://espo.nasa.gov/korus-aq/content/KORUS-AQ_White_Paper)

Arellano, A. F., Kasibhatla, P. S., Giglio, L., Van der Werf, G. R., & Randerson, J. T. (2004). Top-down estimates of global CO sources using MOPITT measurements. *Geophysical research letters*, *31*(1).

Arellano, A. F., Kasibhatla, P. S., Giglio, L., Van der Werf, G. R., Randerson, J. T., & Collatz, G. J. (2006). Time-dependent inversion estimates of global biomass-burning CO emissions using Measurement of Pollution in the Troposphere (MOPITT) measurements. *Journal of Geophysical Research*, *111*, D09303. https://doi.org/10.1029/2005JD006613

Bakwin, P. S., Tans, P. P., & Novelli, P. C. (1994). Carbon monoxide budget in the Northern Hemisphere. *Geophysical Research Letters*, *21*, 433–436.

Barletta, B., Meinardi, S., Simpson, I. J., Atlas, E. L., Beyersdorf, A. J., Baker, A. K., et al. (2009). Characterization of volatile organic compounds (VOCs) in Asian and north American pollution plumes during INTEX-B: Identification of specific Chinese air mass tracers. *Atmospheric Chemistry and Physics*, *9*(14), 5371–5388.

Bey, I., Jacob, D. J., Yantosca, R. M., Logan, J. A., Field, B. D., Fiore, A. M., et al. (2001). Global modeling of tropospheric chemistry with assimilated meteorology: Model description and evaluation. *Journal of Geophysical Research*, *106*(D19), 23,073–23,095.

Blake, D. R., Chen, T. Y., Smith, T. W., Wang, C. J. L., Wingenter, O. W., Blake, N. J., et al. (1996). Three-dimensional distribution of nonmenthane hydrocarbons and halocarbons over the northwestern Pacific during the 1991 Pacific Exploratory Mission (PEM-West A). *Journal of Geophysical Research*, *101*(D1), 1763–1778.

Blake, N. J., Blake, D. R., Simpson, I. J., Lopez, J. P., Johnston, N. A., Swanson, A. L., et al. (2001). Large-scale latitudinal and vertical distributions of NMHCs and selected halocarbons in the troposphere over the Pacific Ocean during the March–April 1999 Pacific Exploratory Mission (PEM-Tropics B). *Journal of Geophysical Research*, *106*(D23), 32,627–32,644. https://doi.org/10.1029/2000JD900773

Blake, N. J., Blake, D. R., Simpson, I. J., Meinardi, S., Swanson, A. L., Lopez, J. P., et al. (2003). NMHCs and halocarbons in Asian continental outflow during the Transport and Chemical Evolution over the Pacific (TRACE-P) Field Campaign: Comparison with PEM-West B. *Journal of Geophysical Research*, *108*, 8806. https://doi.org/10.1029/2002JD003367

Blake, N. J., Streets, D. G., Woo, J. H., Simpson, I. J., Green, J., Meinardi, S., et al. (2004). Carbonyl sulfide and carbon disulfide: Large-scale distributions over the western Pacific and emissions from Asia during TRACE-P. *Journal of Geophysical Research*, *109*, D15S05. https://doi.org/10.1029/2003JD004259

Bogenschutz, P. A., Gettelman, A., Hannay, C., Larson, V. E., Neale, R. B., Craig, C., & Chen, C.-C. (2018). The path to CAM6: Coupled simulations with CAM5.4 and CAM5.5. *Geoscientific Model Development*, *11*, 235–255. https://doi.org/10.5194/gmd-11-235-2018

Bogenschutz, P. A., Gettelman, A., Morrison, H., Larson, V. E., Schanen, D. P., Meyer, N. R., & Craig, C. (2012). Unified parameterization of the planetary boundary layer and shallow convection with a higher-order turbulence closure in the Community Atmosphere Model: Single-column experiments. *Geoscientific Model Development*, *5*(6), 1407.

Brioude, J., Arnold, D., Stohl, A., Cassiani, M., Morton, D., Seibert, P., et al. (2013). The Lagrangian particle dispersion model FLEXPART-WRF version 3.1. *Geoscientific Model Development*, *6*(6), 1889–1904.

Buchholz, R. R., Paton-Walsh, C., Griffith, D. W., Kubistin, D., Caldow, C., Fisher, J. A., et al. (2016). Source and meteorological influences on air quality (CO, CH4 & CO2) at a Southern Hemisphere urban site. *Atmospheric Environment*, *126*, 274–289.

Charlson, R. J., Schwartz, S. E., Hales, J. M., Cess, R. D., Coakley, J. J., Hansen, J. E., & Hofmann, D. J. (1992). Climate forcing by anthropogenic aerosols. *Science*, *255*(5043), 423–430.

Chen, D., Wang, Y., McElroy, M. B., He, K., Yantosca, R. M., & Sager, P. L. (2009). Regional CO pollution and export in China simulated by the high-resolution nested-grid GEOS-Chem model. *Atmospheric Chemistry and Physics*, *9*(11), 3825–3839.

Clappier, A., Belis, C. A., Pernigotti, D., & Thunis, P. (2017). Source apportionment and sensitivity analysis: two methodologies with two different purposes. *Geoscientific Model Development*, *10*(11), 4245.

Deeter, M. N. (2017). *MOPITT (Measurements of Pollution in the Troposphere) version 7 product user's guide*. National Center for Atmospheric Research.

Deeter, M. N., Edwards, D. P., Francis, G. L., Gille, J. C., Martínez-Alonso, S., Worden, H. M., & Sweeney, C. (2017). A climate-scale satellite record for carbon monoxide: The MOPITT Version 7 product. *Atmospheric Measurement Techniques*, *10*(7), 2533.

Deeter, M. N., Edwards, D. P., Gille, J. C., & Worden, H. M. (2015). Information content of MOPITT CO profile retrievals: Temporal and geographical variability. *Journal of Geophysical Research: Atmospheres*, *120*, 12723–12738.

Dennis, J. M., Edwards, J., Evans, K. J., Guba, O., Lauritzen, P. H., Mirin, A. A., et al. (2012). CAM-SE: A scalable spectral element dynamical core for the Community Atmosphere Model. *The International Journal of High Performance Computing Applications*, *26*(1), 74–89.

Doney, S. C., Mahowald, N., Lima, I., Feely, R. A., Mackenzie, F. T., Lamarque, J. F., & Rasch, P. J. (2007). Impact of anthropogenic atmospheric nitrogen and sulfur deposition on ocean acidification and the inorganic carbon system. *Proceedings of the National Academy of Sciences*, *104*(37), 14,580–14,585.

Duncan, B. N., & Bey, I. (2004). A modeling study of the export pathways of pollution from Europe: Seasonal and interannual variations (1987–1997). *Journal of Geophysical Research*, *109*, D08301. https://doi.org/10.1029/2003JD004079

Emmons, L. K., Hess, P. G., Lamarque, J. F., & Pfister, G. G. (2012). Tagged ozone mechanism for MOZART-4, CAM-chem and other chemical transport models. *Geoscientific Model Development*, *5*(6), 1531.

Feely, R. A., Sabine, C. L., Lee, K., Berelson, W., Kleypas, J., Fabry, V. J., & Millero, F. J. (2004). Impact of anthropogenic CO2 on the CaCO3 system in the oceans. *Science*, *305*(5682), 362–366.

Fisher, J. A., Murray, L. T., Jones, D. B. A., & Deutscher, N. M. (2017). Improved method for linear carbon monoxide simulation and source attribution in atmospheric chemistry models illustrated using GEOS-Chem v9. *Geoscientific Model Development*, *10*, 4129–4144. https://doi.org/10.5194/gmd-10-4129-2017

Flemming, J., Benedetti, A., Inness, A., Engelen, R. J., Jones, L., Huijnen, V., et al. (2017). The CAMS interim reanalysis of carbon monoxide, ozone and aerosol for 2003–2015. *Atmospheric Chemistry and Physics*, *17*(3), 1945.

Fuelberg, H. E., Kiley, C. M., Hannan, J. R., Westberg, D. J., Avery, M. A., & Newell, R. E. (2003). Meteorological conditions and transport pathways during the Transport and Chemical Evolution over the Pacific (TRACE-P) experiment. *Journal of Geophysical Research*, *108*, D11205. https://doi.org/10.1029/2002JD003092

Gamnitzer, U., Karstens, U., Kromer, B., Neubert, R. E., Meijer, H. A., Schroeder, H., & Levin, I. (2006). Carbon monoxide: A quantitative tracer for fossil fuel CO2? *Journal of Geophysical Research*, *111*, D22302. https://doi.org/10.1029/2005JD006966

Gao, M., Saide, P. E., Xin, J., Wang, Y., Liu, Z., Wang, Y., et al. (2017). Estimates of health impacts and radiative forcing in winter haze in eastern China through constraints of surface PM2. 5 predictions. *Environmental Science & Technology*, *51*(4), 2178–2185.

Gaubert, B., Arellano, A. F., Barré, J., Worden, H. M., Emmons, L. K., Tilmes, S., et al. (2016). Toward a chemical reanalysis in a coupled chemistry climate model: An evaluation of MOPITT CO assimilation and its impact on tropospheric composition. *Journal of Geophysical Research: Atmospheres*, *121*, 7310–7343. https://doi.org/10.1002/2016JD024863

Gaubert, B., Worden, H. M., Arellano, A. F. J., Emmons, L. K., Tilmes, S., Barré, J., et al. (2017). Chemical feedback from decreasing carbon monoxide emissions. *Geophysical Research Letters*, *44*, 9985–9995. https://doi.org/10.1002/2017GL074987

Gelaro, R., McCarty, W., Suárez, M. J., Todling, R., Molod, A., Takacs, L., et al. (2017). The modern-era retrospective analysis for research and applications, version 2 (MERRA-2). *Journal of Climate*, *30*(14), 5419–5454.

Granier, C., Mueller, J. F., Pétron, G., & Brasseur, G. (1999). A three-dimensional study of the global CO budget. *Chemosphere-Global Change Science*, *1*(1), 255–261.

Grell, G. A., Peckham, S. E., Schmitz, R., McKeen, S. A., Frost, G., Skamarock, W. C., & Eder, B. (2005). Fully coupled "online" chemistry within the WRF model. *Atmospheric Environment*, *39*(37), 6957–6975.

Heald, C. L., Jacob, D. J., Fiore, A. M., Emmons, L. K., Gille, J. C., Deeter, M. N., et al. (2003). Asian outflow and trans-Pacific transport of carbon monoxide and ozone pollution: An integrated satellite, aircraft, and model perspective. *Journal of Geophysical Research*, *108*, 4804. https://doi.org/10.1029/2003JD003507

Heald, C. L., Jacob, D. J., Jones, D., Palmer, P. I., Logan, J. A., Streets, D. G., et al. (2004). Comparative inverse analysis of satellite (MOPITT) and aircraft (TRACE-P) observations to estimate Asian sources of carbon monoxide. *Journal of Geophysical Research*, *109*, D23306. https://doi.org/10.1029/2004JD005185

Heald, C. L., Jacob, D. J., Park, R. J., Alexander, B., Fairlie, T. D., Yantosca, R. M., & Chu, D. A. (2006). Transpacific transport of Asian anthropogenic aerosols and its impact on surface air quality in the United States. *Journal of Geophysical Research*, *111*, D14310. https://doi.org/10.1029/2005JD006847

Hoell, J. M., Davis, D. D., Liu, S. C., Newell, R. E., Akimoto, H., McNeal, R. J., & Bendura, R. J. (1997). The Pacific exploratory mission-west phase B: February–March, 1994. *Journal of Geophysical Research*, *102*(D23), 28,223–28,239.

Hoesly, R. M., Smith, S. J., Feng, L., Klimont, Z., Janssens-Maenhout, G., Pitkanen, T., et al. (2017). Historical (1750–2014) anthropogenic emissions of reactive gases and aerosols from the Community Emission Data System (CEDS). *Geoscientific Model Development Discussions*, 1–41.

Huebert, B. J., Bates, T., Russell, P. B., Shi, G., Kim, Y. J., Kawamura, K., et al. (2003). An overview of ACE-Asia: Strategies for quantifying the relationships between Asian aerosols and their climatic impacts. *Journal of Geophysical Research*, *108*, 8633. https://doi.org/10.1029/2003JD003550

Hurrell, J. W., Holland, M. M., Gent, P. R., Ghan, S., Kay, J. E., Kushner, P. J., et al. (2013). The Community Earth System model: A framework for collaborative research. *Bulletin of the American Meteorological Society*, *94*(9), 1339–1360.

Jacob, D. J., Crawford, J. H., Kleb, M. M., Connors, V. S., Bendura, R. J., Raper, J. L., et al. (2003). Transport and Chemical Evolution over the Pacific (TRACE-P) aircraft mission: Design, execution, and first results. *Journal of Geophysical Research*, *108*, 9000.

Jacob, D. J., Logan, J. A., & Murti, P. P. (1999). Effect of rising Asian emissions on surface ozone in the United States. *Geophysical Research Letters*, *26*(14), 2175–2178.

Jaffe, D., Anderson, T., Covert, D., Kotchenruther, R., Trost, B., Danielson, J., et al. (1999). Transport of Asian air pollution to North America. *Geophysical Research Letters*, *26*(6), 711–714.

Janssens-Maenhout, G., Crippa, M., Guizzardi, D., Dentener, F., Muntean, M., Pouliot, G., et al., 2015. HTAP_v2. 2: A mosaic of regional and global emission grid maps for 2008 and 2010 to study hemispheric transport of air pollution. *Atmospheric Chemistry and Physics*, *15*(19), 11,411–11,432.

Jiang, Z., Worden, J., Worden, H., Deeter, M., Jones, D., Arellano, A., & Henze, D. (2017). Fifteen-year CO emission estimates constrained with MOPITT CO measurements. *Atmospheric Chemistry and Physics*, *17*, 4565–4583. https://doi.org/10.5194/acp-17-4565-2017

Jiang, Z., Worden, J. R., Payne, V. H., Zhu, L., Fischer, E., Walker, T., & Jones, D. (2016). Ozone export from East Asia: The role of PAN. *Journal of Geophysical Research: Atmospheres*, *121*, 6555–6563.

Kanaya, Y., Pan, X., Miyakawa, T., Komazaki, Y., Taketani, F., Uno, I., & Kondo, Y. (2016). Long-term observations of black carbon mass concentrations at Fukue Island, western Japan, during 2009–2015: Constraining wet removal rates and emission strengths from East Asia. *Atmospheric Chemistry and Physics*, *16*(16), 10,689–10,705.

Kennedy, C. A., Stewart, I., Facchini, A., Cersosimo, I., Mele, R., Chen, B., et al. (2015). Energy and material flows of megacities. *Proceedings of the National Academy of Sciences*, *112*(19), 5985–5990.

Lamarque, J. F., Emmons, L. K., Hess, P. G., Kinnison, D. E., Tilmes, S., Vitt, F., et al. (2012). CAM-chem: Description and evaluation of interactive atmospheric chemistry in the Community Earth System Model. *Geoscientific Model Development*, *5*(2), 369.

Li, M., Zhang, Q., Kurokawa, J.-I., Woo, J.-H., He, K., Lu, Z., et al. (2017). MIX: A mosaic Asian anthropogenic emission inventory under the international collaboration framework of the MICS-Asia and HTAP. *Atmospheric Chemistry and Physics*, *17*, 935–963. https://doi.org/10.5194/acp-17-935-2017

Li, Q., Jacob, D. J., Bey, I., Palmer, P. I., Duncan, B. N., Field, B. D., et al. (2002). Transatlantic transport of pollution and its effects on surface ozone in Europe and North America. *Journal of Geophysical Research*, *107*, 4370. https://doi.org/10.1029/2001JD001422

Liang, Q., Jaeglé, L., Jaffe, D. A., Weiss-Penzias, P., Heckman, A., & Snow, J. A. (2004). Long-range transport of Asian pollution to the northeast Pacific: Seasonal variations and transport pathways of carbon monoxide. *Journal of Geophysical Research*, *109*, D23S0. https://doi.org/10.1029/2003JD004402

Liu, H., Jacob, D. J., Bey, I., Yantosca, R. M., Duncan, B. N., & Sachse, G. W. (2003). Transport pathways for Asian pollution outflow over the Pacific: Interannual and seasonal variations. *Journal of Geophysical Research*, *108*, D22301. https://doi.org/10.1029/2002JD003102

Liu, X., Ma, P.-L., Wang, H., Tilmes, S., Singh, B., Easter, R. C., et al. (2016). Description and evaluation of a new four-mode version of the Modal Aerosol Module (MAM4) within version 5.3 of the Community Atmosphere Model. *Geoscientific Model Development*, *9*, 505–522, https://doi.org/10.5194/gmd-9-505-2016

Maher, B. A., Ahmed, I. A., Karloukovski, V., MacLaren, D. A., Foulds, P. G., Allsop, D., et al. (2016). Magnetite pollution nanoparticles in the human brain. *Proceedings of the National Academy of Sciences*, *113*(39), 10,797–10,801.

Miyazaki, K., Eskes, H., Sudo, K., Boersma, K. F., Bowman, K., & Kanaya, Y. (2017). Decadal changes in global surface NOx emissions from multi-constituent satellite data assimilation. *Atmospheric Chemistry And Physics*, *17*, 807–837. https://doi.org/10.5194/acp-17-807-2017

Miyazaki, K., Sekiya, T., Fu, D., Bowman, K. W., Kulawik, S. S., Sudo, K., et al. (2018). Balance of emission and dynamical controls on ozone during KORUS-AQ from multi-constituent satellite data assimilation. *Journal of Geophysical Research: Atmospheres*.

Molod, A., Takacs, L., Suarez, M., & Bacmeister, J. (2015). Development of the GEOS-5 atmospheric general circulation model: Evolution from MERRA to MERRA2. *Geoscientific Model Development*, *8*(5), 1339.

Monks, S. A., Arnold, S. R., Emmons, L. K., Law, K. S., Turquety, S., Duncan, B. N., et al. (2015). Multi-model study of chemical and physical controls on transport of anthropogenic and biomass burning pollution to the Arctic. *Atmospheric Chemistry and Physics*, *15*(6), 3575–3603.

Morrison, H., & Gettelman, A. (2008). A new two-moment bulk stratiform cloud microphysics scheme in the Community Atmosphere Model, version 3 (CAM3). Part I: Description and numerical tests. *Journal of Climate*, *21*(15), 3642–3659.

Müller, J. F., Stavrakou, T., Bauwens, M., George, M., Hurtmans, D., Coheur, P. F., et al. (2018). Top-down CO emissions based on IASI observations and hemispheric constraints on OH levels. *Geophysical Research Letters*, *45*(3), 1621–1629.

Naik, V., Voulgarakis, A., Fiore, A. M., Horowitz, L. W., Lamarque, J. F., Lin, M., et al. (2013). Preindustrial to present-day changes in tropospheric hydroxyl radical and methane lifetime from the Atmospheric Chemistry and Climate Model Intercomparison Project (ACCMIP). *Atmospheric Chemistry and Physics*, *13*(10), 5277–5298.

Ohara, T. A. H. K., Akimoto, H., Kurokawa, J. I., Horii, N., Yamaji, K., Yan, X., & Hayasaka, T. (2007). An Asian emission inventory of anthropogenic emission sources for the period 1980–2020. *Atmospheric Chemistry and Physics*, *7*(16), 4419–4444.

Palmer, P. I., Jacob, D. J., Mickley, L. J., Blake, D. R., Sachse, G. W., Fuelberg, H. E., & Kiley, C. M. (2003). Eastern Asian emissions of anthropogenic halocarbons deduced from aircraft concentration data. *Journal of Geophysical Research*, *108*(D24), 4753. https://doi.org/10.1029/2003JD003591

Park, M., Randel, W. J., Emmons, L. K., & Livesey, N. J. (2009). Transport pathways of carbon monoxide in the Asian summer monsoon diagnosed from Model of Ozone and Related Tracers (MOZART). *Journal of Geophysical Research*, *114*, D08303. https://doi.org/10.1029/2008JD010621

Parrish, D. D., Trainer, M., Hereid, D., Williams, E. J., Olszyna, K. J., Harley, R. A., et al. (2002). Decadal change in carbon monoxide to nitrogen oxide ratio in US vehicular emissions. *Journal of Geophysical Research*, *107*, 4140. https://doi.org/10.1029/2001JD000720

Pétron, G., Granier, C., Khattatov, B., Yudin, V., Lamarque, J. F., Emmons, L., et al. (2004). Monthly CO surface sources inventory based on the 2000–2001 MOPITT satellite data. *Geophysical Research Letters*, *31*, L21107. https://doi.org/10.1029/2004GL020560

Pfister, G., Petron, G., Emmons, L. K., Gille, J. C., Edwards, D. P., Lamarque, J. F., et al. (2004). Evaluation of CO simulations and the analysis of the CO budget for Europe. *Journal of Geophysical Research*, *109*, D19304. https://doi.org/10.1029/2004JD004691

Pfister, G. G., Avise, J., Wiedinmyer, C., Edwards, D. P., Emmons, L. K., Diskin, G. D., et al. (2011). CO source contribution analysis for California during ARCTAS-CARB. *Atmospheric Chemistry and Physics*, *11*, 7515–7532. https://doi.org/10.5194/acp-11-7515-2011

Pfister, G. G., Reddy, P. J., Barth, M. C., Flocke, F. F., Fried, A., Herndon, S. C., et al. (2017). Using observations and source-specific model tracers to characterize pollutant transport during FRAPPÉ and DISCOVER-AQ. *Journal of Geophysical Research: Atmospheres*, *122*, 10,474–10,502. https://doi.org/10.1002/2017JD027257

Protonotariou, A. P., Kostopoulou, E., Tombrou, M., & Giannakopoulos, C. (2013). European CO budget and links with synoptic circulation based on GEOS-CHEM model simulations. *Tellus B: Chemical and Physical Meteorology*, *65*(1), 18640.

Qin, D. (2007). Decline in the concentrations of chlorofluorocarbons (CFC-11, CFC-12 and CFC-113) in an urban area of Beijing, China. *Atmospheric Environment*, *41*, 8424–8430.

Rienecker, M. M., Suarez, M. J., Gelaro, R., Todling, R., Bacmeister, J., Liu, E., et al. (2011). MERRA: NASA's modern-era retrospective analysis for research and application. *Journal of Climate*, *24*, 3624–3648. https://doi.org/10.1175/JCLI-D-11-00015.1

Seibert, P., & Frank, A. (2004). Source-receptor matrix calculation with a Lagrangian particle dispersion model in backward mode. *Atmospheric Chemistry and Physics*, *4*(1), 51–63.

Shindell, D. T., Faluvegi, G., Stevenson, D. S., Krol, M. C., Emmons, L. K., Lamarque, J. F., et al. (2006). Multimodel simulations of carbon monoxide: Comparison with observations and projected near-future changes. *Journal of Geophysical Research*, *111*.

Shindell, D., Faluvegi, G., Walsh, M., Anenberg, S. C., Van Dingenen, R., Muller, N. Z., et al. (2011). Climate, health, agricultural and economic impacts of tighter vehicle-emission standards. *Nature Climate Change*, *1*(1), 59–66.

Silva, S. J., Arellano, A. F., & Worden, H. M. (2013). Toward anthropogenic combustion emission constraints from space-based analysis of urban CO_2/CO sensitivity. *Geophysical Research Letters*, *40*, 4971–4976.

Smith, R. J. (2009). Use and misuse of the reduced major axis for line-fitting. *American Journal of Physical Anthropology*, *140*(3), 476–486.
Staudt, A. C., Jacob, D. J., Logan, J. A., Bachiochi, D., Krishnamurti, T. N., & Sachse, G. W. (2001). Continental sources, transoceanic transport, and interhemispheric exchange of carbon monoxide over the Pacific. *Journal of Geophysical Research*, *106*, 32571–32589. https://doi.org/10.1029/2001JD900078
Stein, O., Schultz, M. G., Bouarar, I., Clark, H., Huijnen, V., Gaudel, A., et al. (2014). On the wintertime low bias of Northern Hemisphere carbon monoxide found in global model simulations. *Atmospheric Chemistry and Physics*, *14*, 9295–9316.
Stohl, A., Eckhardt, S., Forster, C., James, P., Spichtinger, N., & Seibert, P. (2002). A replacement for simple back trajectory calculations in the interpretation of atmospheric trace substance measurements. *Atmospheric Environment*, *36*, 4635–4648.
Stohl, A., Forster, C., Frank, A., Seibert, P., & Wotawa, G. (2005). The Lagrangian particle dispersion model FLEXPART version 6.2. *Atmospheric Chemistry and Physics*, *5*, 2461–2474. https://doi.org/10.5194/acp-5-2461-2005
Streets, D. G., Zhang, Q., Wang, L., He, K., Hao, J., Wu, Y., et al. (2006). Revisiting China's CO emissions after the transport and chemical evolution over the Pacific (TRACE-P) mission: Synthesis of inventories, atmospheric modeling, and observations. *Journal of Geophysical Research*, *111*, D14306. https://doi.org/10.1029/2006JD007118
Strode, S. A., Duncan, B. N., Yegorova, E. A., Kouatchou, J., Ziemke, J. R., & Douglass, A. R. (2015). Implications of carbon monoxide bias for methane lifetime and atmospheric composition in chemistry climate models. *Atmospheric Chemistry and Physics*, *15*, 11789–11805. https://doi.org/10.5194/acp-15-11789-2015
Tang, W., & Arellano, A. F. (2017). Investigating dominant characteristics of fires across the Amazon during 2005–2014 through satellite data synthesis of combustion signatures. *Journal of Geophysical Research: Atmospheres*, *122*, 1224–1245. https://doi.org/10.1002/2016JD025216
Tang, W., Arellano, A. F., DiGangi, J. P., Choi, Y., Diskin, G. S., Agustí-Panareda, A., et al. (2018). Evaluating high-resolution forecasts of atmospheric CO and CO_2 from a global prediction system during KORUS-AQ field campaign. *Atmospheric Chemistry and Physics*, *18*, 11007–11030. https://doi.org/10.5194/acp-18-11007-2018
Taylor, K. E. (2001). Summarizing multiple aspects of model performance in a single diagram. *Journal of Geophysical Research*, *106*(1755), 7183–7192. https://doi.org/10.1029/2000JD900719
Tilmes, S., Lamarque, J. F., Emmons, L. K., Kinnison, D. E., Ma, P. L., Liu, X., et al. (2015). Description and evaluation of tropospheric chemistry and aerosols in the Community Earth System Model (CESM1. 2). *Geoscientific Model Development*, *8*, 1395–1426.
Turnbull, J. C., Tans, P. P., Lehman, S. J., Baker, D., Conway, T. J., Chung, Y. S., et al. (2011). Atmospheric observations of carbon monoxide and fossil fuel CO_2 emissions from East Asia. *Journal of Geophysical Research*, *116*, D24306. https://doi.org/10.1029/2011JD016691
Valari, M., & Menut, L. (2008). Does an increase in air quality models' resolution bring surface ozone concentrations closer to reality?. *Journal of Atmospheric and Oceanic Technology*, *25*(11), 1955–1968. https://doi.org/10.1175/2008jtecha1123.1
Vay, S. A., Choi, Y., Vadrevu, K. P., Blake, D. R., Tyler, S. C., Wisthaler, A., et al. (2011). Patterns of CO_2 and radiocarbon across high northern latitudes during International Polar Year 2008. *Journal of Geophysical Research*, *116*, D1430. https://doi.org/10.1029/2011JD015643
Wang, Y., Choi, Y., Zeng, T., Ridley, B., Blake, N., Blake, D., & Flocke, F. (2006). Late-spring increase of trans-Pacific pollution transport in the upper troposphere. *Geophysical Research Letters*, *33*, L01811. https://doi.org/10.1029/2005GL024975
Wang, Y., Munger, J. W., Xu, S., McElroy, M. B., Hao, J., Nielsen, C. P., & Ma, H. (2010). CO_2 and its correlation with CO at a rural site near Beijing: Implications for combustion efficiency in China. *Atmospheric Chemistry and Physics*, *10*(18), 8881–8897.
Warner, J. X., Wei, Z., Strow, L. L., Barnet, C. D., Sparling, L. C., Diskin, G., & Sachse, G. (2010). Improved agreement of AIRS tropospheric carbon monoxide products with other EOS sensors using optimal estimation retrievals. *Atmospheric Chemistry and Physics*, *10*(19), 9521–9533.
Wiedinmyer, C., Akagi, S. K., Yokelson, R. J., Emmons, L. K., Al-Saadi, J. A., Orlando, J. J., & Soja, A. J. (2011). The Fire INventory from NCAR (FINN): A high resolution global model to estimate the emissions from open burning. *Geoscientific Model Development*, *4*(3), 625.
Wild, O., & Prather, M. J. (2006). Global tropospheric ozone modeling: Quantifying errors due to grid resolution. *Journal of Geophysical Research*, *111*, D1130. https://doi.org/10.1029/2005JD006605
Woo, J. H., Streets, D. G., Carmichael, G. R., Tang, Y. H., Yoo, B., Lee, W. C., et al. (2003). Contribution of biomass and biofuel emissions to trace gas distributions in Asia during the TRACE-P experiment. *Journal of Geophysical Research*, *108*, 8812. https://doi.org/10.1029/2002JD003200
Worden, H. M., Deeter, M. N., Edwards, D. P., Gille, J. C., Drummond, J. R., & Nédélec, P. (2010). Observations of near-surface carbon monoxide from space using MOPITT multispectral retrievals. *Journal of Geophysical Research*, *115*, D18314. https://doi.org/10.1029/2010JD014242
Xue, L., Wang, T., Simpson, I. J., Ding, A., Gao, J., Blake, D. R., et al. (2011). Vertical distributions of non-methane hydrocarbons and halocarbons in the lower troposphere over northeast China. *Atmospheric environment*, *45*(36), 6501–6509.
Yan, Y., Lin, J., Chen, J., & Hu, L. (2016). Improved simulation of tropospheric ozone by a global-multi-regional two-way coupling model system. *Atmospheric Chemistry and Physics*, *16*, 2381–2400, https://doi.org/10.5194/acp-16-2381-2016.
Yin, Y., Chevallier, F., Ciais, P., Broquet, G., Fortems-Cheiney, A., Pison, I., & Saunois, M. (2015). Decadal trends in global CO emissions as seen by MOPITT. *Atmospheric Chemistry & Physics Discussions*, *15*(10).
Yu, K., Jacob, D. J., Fisher, J. A., Kim, P. S., Marais, E. A., Miller, C. C., et al. (2016). Sensitivity to grid resolution in the ability of a chemical transport model to simulate observed oxidant chemistry under high-isoprene conditions. *Atmospheric Chemistry and Physics*, *16*(7), 4369–4378.